31st Annual International Conference of the IEEE EMBS
Minneapolis, Minnesota, USA, September 2-6, 2009

Macroscopic Two-Pump Two-Vasculature Cardiovascular Model to Support Treatment of Acute Heart Failure

Masaru Sugimachi, *Member, IEEE*, Kenji Sunagawa, *Member, IEEE*,
Kazunori Uemura, Atsunori Kamiya, Shuji Shimizu, Masashi Inagaki and Toshiaki Shishido

Abstract— **Comprehensive understanding of hemodynamics remains a challenge even for expert cardiologists, partially due to a lack of an appropriate macroscopic model. We attempted to amend three major problems of Guyton's conceptual model (unknown left atrial pressure, unilateral heart damage, blood redistribution) and developed a comprehensive macroscopic model of hemodynamics that provides quantitative information. We incorporated a third axis of left atrial pressure, resulting in a 3D coordinate system. Pump functions of left and right heart are expressed by an integrated cardiac output curve, and the capacitive function of total vasculature by a venous return surface. The equations for both the cardiac output curve and venous return surface would facilitate precise diagnosis (especially evaluation of blood volume) and choice of appropriate treatments, including application to autopilot systems.**

I. Introduction

COMPREHSNSIVE understanding of hemodynamics remains a challenge even for specialist clinicians including cardiologists. This is in part attributed to a lack of an appropriate macroscopic model of hemodynamics that would facilitate reasoning. Most cardiologists relied only on, if at all, the classical Guyton's circulatory equilibrium framework [1].

Guyton's model consists of only two subdivisions of the whole circulation: the cardiopulmonary component (in which both hearts and pulmonary vasculature are lumped) and the systemic vascular bed. These two subdivisions are characterized by the 'cardiac output curve' and 'venous return curve', respectively. The 'cardiac output curve' approximated the (total) pump function, and the 'venous return curve' approximated the capacitive function of systemic vasculature. The intersection of these curves coincides with the operating point of the circulation.

Guyton's model is, however, inappropriate (see MODEL AND METHODS) for the understanding of hemodynamics in patients with, for example, acute myocardial infarction, where only one ventricle is preferentially damaged. That is why many cardiologists gradually abandoned using Guyton's model for their reasoning.

If we can amend the shortcomings of Guyton's model and develop a more appropriate model, the new model would obviously help diagnosis procedures and treatment selection. Furthermore, the model may be able to quantify the hemodynamic abnormalities rather than just to identify them.

Therefore, the aim of this study was to develop a comprehensive macroscopic model of hemodynamics that would provide quantitative information and aid diagnosis and treatments.

Manuscript received April 7, 2009. This work was supported in part by Grant-in-Aid for Scientific Research (B 20300164, C 20500404) from the Ministry of Education, Culture, Sports, Science and Technology, by Health and Labour Sciences Research Grants (H19-nano-ippan-009, H20-katsudo -shitei-007) from the Ministry of Health Labour and Welfare of Japan.

M. Sugimachi, K. Uemura, A. Kamiya, S. Shimizu, M. Inagaki and T. Shishido are with the National Cardiovascular Center Research Institute, Suita, Osaka 5658565, Japan (corresponding author Masaru Sugimachi to provide phone: +81-6-6833-512; fax: +81-6-6835-5403; e-mail: su91mach@ri.ncvc.go.jp).

K. Sunagawa is with Kyushu University, Fukuoka 8128582 Japan. (e-mail: sunagawa@cardiol med.kyushu-u.ac.jp).

II. Model and Methods

A. Shortcomings of Guyton's Model

Guyton's model has a number of problems when used in patients with unilateral heart failure.

First, the model does not provide left atrial pressure (LAP) values directly. LAP indicates the degree of pulmonary congestion and blood desaturation, and is as important as cardiac output (CO) and blood pressure.

Second, it is impossible to precisely model unilateral heart failure, which is frequently seen in patients with ischemic heart disease.

Third, in unilateral heart failure, the relative blood volumes in pulmonary and systemic vascular beds vary. As Guyton's model assumes only blood volume within the systemic vascular bed, such redistribution would shift the venous return curve even though the total blood volume remains the same.

B. Development of Comprehensive Cardiovascular Model

To solve the above problems, we extended Guyton's model.

First, a third axis of LAP was introduced in our new model (Fig. 1) [2], [3], so that LAP can be obtained directly. The pumping ability of the heart and the capacitive function of the vasculature are expressed simultaneously in the 3D space (RAP-LAP-CO coordinate system).

Second, the pumping abilities of the left and right heart are expressed separately by the respective cardiac output surfaces that are independent of each other. In an equilibrium state, by matching the cardiac output of both sides, the pumping ability of the whole heart can be integrated and expressed by a curve

expressing the intersection of the two surfaces (integrated cardiac output curve, Fig. 1, thick curve).

Third, the capacitive function of total vasculature (including both systemic and pulmonary vasculatures) is expressed by the venous return surface (Fig. 1, shaded surface), which is an extension of the venous return curve. This surface expresses the changes in LAP and right atrial pressure (RAP) in response to CO change, while the total intravascular blood volume remains constant. In addition, blood redistribution between systemic and pulmonary vasculatures (without change in total blood volume) will be expressed by movement within the surface rather than by deviation from the surface.

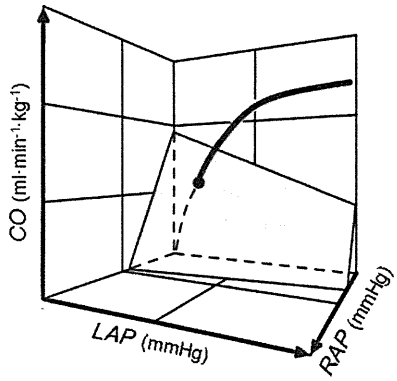

Fig. 1. An original macroscopic model of hemodynamics (an extended Guyton's model). The curve expresses the integrated pumping ability of left and right heart. The shaded surface characterizes the capacitive function of the total (systemic + pulmonary) vasculatures. The surface remains constant as long as the total intravascular blood volume remains the same. CO, cardiac output; LAP, left atrial pressure; RAP, right atrial pressure.

C. Animal Experiments to Characterize Venous Return Surface

Figure 2 depicts the scheme of an experiment to characterize the venous return surface. We replaced the left and right heart with roller pumps, which allows us to change CO of the right heart or left heart independently.

By adjusting the flow (i.e., CO) of the two pumps to the same level, the changes in RAP and LAP in response to a change in CO can be observed. Blood redistribution between systemic and pulmonary vasculatures can be reproduced by transiently unbalancing the flow of the two pumps.

From each dog (n = 6), we obtained 6 different sets of data (CO, RAP, LAP). These data were subjected to bivariate linear regression using RAP and LAP as independent variables and CO as the dependent variable.

III. Results

Figure 3 illustrates the venous return surfaces obtained from 6 dogs. Bivariate linear regression in each animal yielded a flat surface in 3D space. The surface is shown as a line in Fig. 3, because we have projected the surface in a

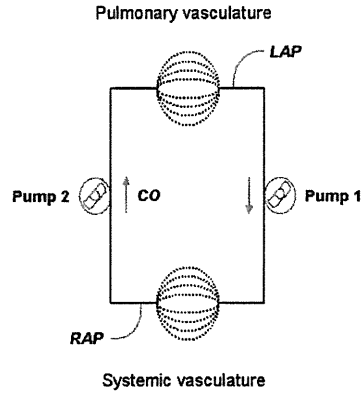

Fig. 2. An experimental scheme to characterize venous return surface. By replacing the left and right heart with roller pumps, one can change cardiac output of the right heart or left heart independently.

direction parallel to the surface. The experimental data obtained from each of the 6 animals showed good fit with the surface. In addition, the surfaces obtained from 6 animals were almost parallel, as shown by the nearly parallel 3D coordinate axes. These experimental results indicated that the venous return surface is linear and can be expressed by a common equation for all animals.

Further, by infusing or withdrawing known amounts of blood, we were able to derive an equation for the venous return surface as follows:

$$CO = V / 0.129 - 19.61\ RAP - 3.49\ LAP$$

where V is total intravascular stressed blood volume. This formula [$V = (CO + 19.61\ RAP + 3.49\ LAP) \times 0.129$] can be used to quantify V from CO, RAP and LAP.

We also succeeded to quantify the integrated cardiac output curve by logarithmic functions as follows:

$$CO = S_L\ [\ln(LAP-2.03)+0.80]$$

$$CO = S_R\ [\ln(RAP-2.13)+1.90]$$

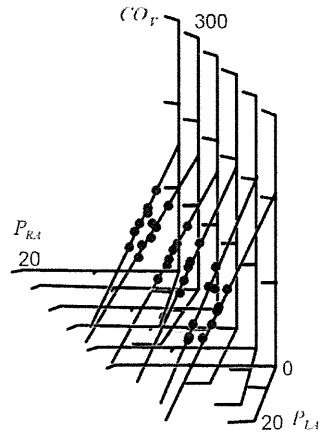

Fig. 3. Superimposed venous return surfaces obtained from 6 dogs. For each dog, the venous return surface (RAP-LAP-CO relationship) in 3D coordinate system was projected in a direction parallel to the surface, and was superimposed with each other.

where S_L and S_R are parameters expressing the pumping ability of the left and right heart, respectively. These equations are also useful for quantifying the pumping ability of right and left heart (S_L = CO / [ln(LAP - 2.03) + 0.80], S_R = CO / [ln(RAP - 2.13) + 1.90]).

Using this model, we are able to predict with acceptable precision the hemodynamics after infusion or withdrawal of known amounts of blood (CO: y = 0.93x + 6.5, r^2 = 0.96, SEE = 7.5 ml·min^{-1}·kg^{-1}; LAP: y = 0.90x + 0.5, r^2= 0.93, SEE = 1.4 mmHg; RAP: y = 0.87x + 0.4, r^2= 0.91, SEE = 0.4 mmHg) (Fig. 4) [3].

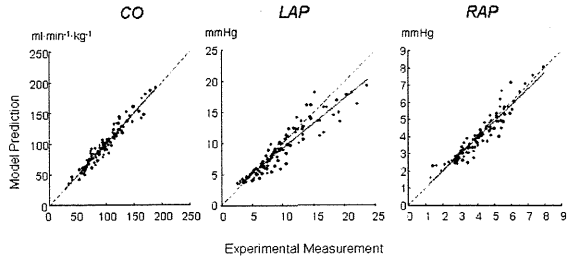

Fig. 4. Prediction of CO, LAP, and RAP based on our comprehensive macroscopic model of hemodynamics.

IV. Discussion

A. Difficulty in Decision Making of Heart Failure Treatment

Three hemodynamic variables: blood pressure, CO and LAP, appear to be the most essential factors influencing the survival of patients with heart failure. Our model clearly indicates that pump functions of left and right heart and total intravascular blood volume are determinants of CO and LAP. Systemic vascular resistance is an additional determinant of blood pressure.

For clinicians, the evaluation of blood volume is relatively difficult compared to pump functions and vascular resistance. In practice, clinicians have been using RAP as a proxy for blood volume. It is clear from our results [V = (CO + 19.61 RAP + 3.49 LAP) × 0.129] that blood volume (V) is not solely determined by RAP. Rather, all three parameters of CO, RAP and LAP are necessary to evaluate blood volume. The equation indicates that an increase of RAP by 1 mmHg is equivalent to an LAP increase of 5.6 mmHg, and a CO increase of 19.61 mL/min/kg (ca. 0.98 L/min for a 50-kg patient).

B. Application of the Model: Autopilot System

The biggest benefit of our comprehensive visual model of hemodynamics is that it enables us to diagnose the abnormality of cardiovascular system in a quantitative manner. This would lead to appropriate selection of drugs and their doses.

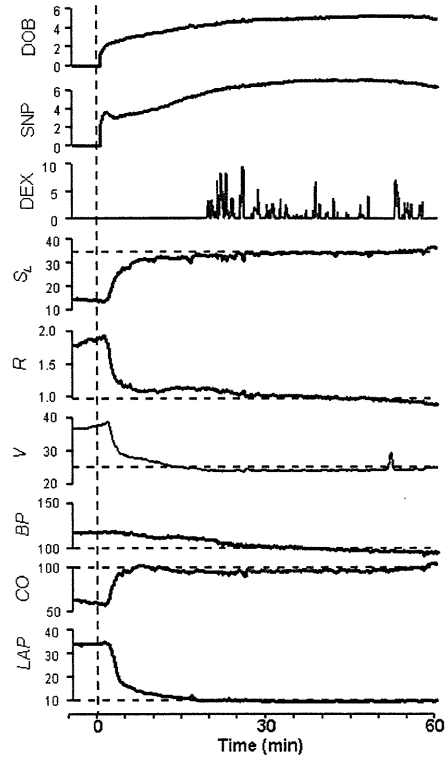

Fig. 5. An example of correction of hemodynamics with an autopilot system. By normalizing cardiovascular properties [pump function (S_L), resistance (R), blood volume (V)] with the administration of dobutamine (DOB), sodium nitroprusside (SNP), and dextran 40 solution (DEX), all the abnormal hemodynamic variables (increased blood pressure [BP], decreased cardiac output [CO], and elevated left atrial pressure [LAP]) were resolved rapidly, sufficiently, and stably.

As shown in Fig. 5, by translating hemodynamic variables into cardiovascular properties (pump function, vascular resistance, and blood volume), and by controlling each of these parameters with individual drug with preferential effect on the parameter, we are able to correct automatically all the parameters of blood pressure, CO and LAP rapidly, stably, and simultaneously.

Using an autopilot system to administer dobutamine (DOB at 5 ± 3 mg·kg^{-1}·min^{-1}), nitroprusside (SNP at 4 ± 2 mg·kg^{-1}·min^{-1}), dextran infusion (DEX at 2 ± 2 ml·kg^{-1}), and furosemide (10 mg in one, 20 mg in one) in 12 dogs with acute heart failure rapidly normalized blood pressure, CO, and LAP in 5 ± 7, 7 ± 5, and 12 ± 10 minutes, respectively. The normalized values remained stable thereafter (RMS values, blood pressure = 4 ± 3 mmHg, CO = 5 ± 2 ml·min^{-1}·kg^{-1}, LAP = 0.8 ± 0.6 mmHg).

V. Conclusion

We have successfully developed a comprehensive macroscopic model of hemodynamics that provides quantitative information. Using a 3D coordinate system, the pump functions of left and right heart are expressed by an

integrated cardiac output curve, and the capacitive function of total vasculature by a venous return surface. The equations of both the cardiac output curve and venous return surface would facilitate accurate diagnosis (especially evaluation of blood volume) and choice of appropriate treatments, including application to autopilot systems.

REFERENCES

[1] A. C. Guyton, "Determination of cardiac output by equating venous return curves with cardiac response curves," *Physiol. Rev.* vol. 35, no. 1,123–129, Jan. 1955.

[2] K. Uemura, M. Sugimachi, T. Kawada, A. Kamiya, Y. Jin, *et al.*, "A novel framework of circulatory equilibrium," *Am. J. Physiol. Heart Circ. Physiol.* vol. 286, no. 6, pp. H2376–H2385, Jun. 2004.

[3] K. Uemura, T. Kawada, A. Kamiya, T. Aiba, I. Hidaka, *et al.*, "Prediction of circulatory equilibrium in response to changes in stressed blood volume," *Am. J. Physiol. Heart Circ. Physiol.* vol. 289, no. 1, H301–H307, Jul. 2005.

Neurochemistry International xxx (2009) xxx–xxx

Contents lists available at ScienceDirect

Neurochemistry International

journal homepage: www.elsevier.com/locate/neuint

Role of Ca^{2+}-activated K^+ channels in catecholamine release from *in vivo* rat adrenal medulla

Tsuyoshi Akiyama [a,*], Toji Yamazaki [a], Toru Kawada [b], Shuji Shimizu [b], Masaru Sugimachi [b], Mikiyasu Shirai [a]

[a] Department of Cardiac Physiology, National Cardiovascular Center Research Institute, 5-7-1 Fujishiro-dai, Suita, 565-8565 Osaka, Japan
[b] Department of Cardiovascular Dynamics, National Cardiovascular Center Research Institute, Suita, 565-8565, Japan

ARTICLE INFO

Article history:
Received 24 September 2009
Received in revised form 21 October 2009
Accepted 28 October 2009
Available online xxx

Keywords:
Anesthetized rats
Microdialysis technique
Acetylcholine
Norepinephrine
Epinephrine
Ca^{2+}-activated K^+ channels

ABSTRACT

To elucidate the role of Ca^{2+}-activated K^+ (K_{Ca}) channels in the presynaptic acetylcholine (ACh) release from splanchnic nerve endings and the postsynaptic catecholamine release from chromaffin cells, we applied microdialysis technique to the left adrenal medulla of anesthetized rats and investigated the effects of local administration of K_{Ca} channel antagonists through dialysis probes on the release of ACh and/or catecholamine, induced by electrical stimulation of splanchnic nerves or local administration of ACh through the dialysis probes. *Nerve stimulation-induced release*: in the presence of a cholinesterase inhibitor, neostigmine, large-conductance K_{Ca} (BK) channel antagonists, iberiotoxin and paxilline enhanced the presynaptic ACh release and postsynaptic norepinephrine (NE) and epinephrine (Epi) release. Small-conductance K_{Ca} (SK) channel antagonists, apamin and scyllatoxin enhanced the Epi release without any changes in ACh or NE release. In the absence of neostigmine, ACh release was not detected. Iberiotoxin and paxilline enhanced NE and Epi release. Apamin and scyllatoxin had no effect on NE or Epi release. *Exogenous ACh-induced release*: iberiotoxin and paxilline enhanced the Epi release, but had no effect on the NE release. Apamin and scyllatoxin enhanced both NE and Epi release. In conclusion, BK channels on splanchnic nerve endings play an inhibitory role in the physiological catecholamine release from adrenal medulla by limiting presynaptic ACh release while SK channels do not. BK channels on Epi-storing cells may play an inhibitory role in nerve stimulation-induced Epi release. SK channels on NE- and Epi-storing cells play a minor role in nerve stimulation-induced catecholamine release.

1. Introduction

The physiological release of catecholamine from adrenal medulla is controlled by central sympathetic neurons through splanchnic nerves. Splanchnic nerve endings make synaptic-like contacts with chromaffin cells (Coupland, 1965). Activation of splanchnic nerve endings causes Ca^{2+} influx through voltage-dependent Ca^{2+} channels, which evokes exocytotic acetylcholine (ACh) release. This ACh release activates cholinergic receptors on chromaffin cells, which causes Ca^{2+} influx through voltage-dependent Ca^{2+} channels and evokes exocytotic catecholamine release from chromaffin cells (García et al., 2006).

Ca^{2+}-activated K^+ (K_{Ca}) currents are consistently found at neuronal cells or nerve terminals (Meir et al., 1999). K_{Ca} channels are located in the vicinity of voltage-dependent Ca^{2+} channels and activated by Ca^{2+} influx through voltage-dependent Ca^{2+} channels. Activation of the K_{Ca} channels induces outward efflux of K^+, causes hyperpolarization of the membrane, and subsequently limits Ca^{2+} entry through voltage-dependent Ca^{2+}channels. Thus, K_{Ca} channels may be present at two different sites in the adrenal medulla: splanchnic nerve endings and chromaffin cells, and are then involved in the physiological regulation of presynaptic ACh release and/or postsynaptic catecholamine release. In fact, it has been reported that K_{Ca} channels on chromaffin cells play an important role in catecholamine release (Montiel et al., 1995; Uceda et al., 1992; Wada et al., 1995). Little information is, however, available on the role of K_{Ca} channels in the presynaptic ACh release from splanchnic nerve endings.

We have recently developed a dialysis technique to simultaneously monitor the release of presynaptic ACh and postsynaptic catecholamine in the *in vivo* adrenal medulla (Akiyama et al., 2004a). This method makes it possible to investigate the functional roles of K_{Ca} channels in the ACh release from splanchnic nerve endings and the catecholamine release from adrenal medulla in the *in vivo* state. In the present study, we applied the microdialysis technique to the adrenal medulla of anesthetized rats and investigated the effects of K_{Ca} channel antagonists on the release of presynaptic ACh and postsynaptic catecholamine.

* Corresponding author. Tel.: +81 6 6833 5012x2380; fax: +81 6 6872 8092.
E-mail address: takiyama@ri.ncvc.go.jp (T. Akiyama).

0197-0186/$ – see front matter © 2009 Elsevier Ltd. All rights reserved.
doi:10.1016/j.neuint.2009.10.010

In electrophysiological studies, K_{Ca} channels can be divided into two types based on their single channel conductance: large-conductance (BK) and small-conductance K_{Ca} (SK) channels (Blatz and Magleby, 1987). We tested two types of BK channel antagonists: the selective peptidergic BK channel antagonist, iberiotoxin (Candia et al., 1992) and the non-peptidergic BK channel antagonist, paxilline (Kanus et al., 1994). Similarly we tested two types of SK channel antagonists: the selective peptidergic SK channel antagonist, apamin (Blatz and Magleby, 1986) and the selective peptidergic SK channel antagonist different in amino acid sequence, scyllatoxin (Auguste et al., 1990).

2. Materials and methods

2.1. Animal preparation

Animal care was provided in strict accordance with the *Guiding Principles for the Care and Use of Animals in the Field of Physiological Sciences* approved by the Physiological Society of Japan. All protocols were approved by the Animal Subject Committee of the National Cardiovascular Center. Adult male Wistar rats weighing 380–460 g were anesthetized with pentobarbital sodium (50–55 mg/kg, i.p.). A cervical midline incision was made to expose the trachea, which was then cannulated. The rats were ventilated with a constant-volume respirator using room air mixed with oxygen. The left femoral artery and vein were cannulated for monitoring arterial blood pressure and administration of anesthetic, respectively. The level of anesthesia was maintained with a continuous intravenous infusion of pentobarbital sodium (15–25 mg/kg/h, i.v.). The electrocardiogram was monitored to record the heart rate. A thermostatic heating pad was used to keep the esophageal temperature within a range of 37–38 C. With the animal in the lateral position, the left adrenal gland and left splanchnic nerve were exposed by a subcostal flank incision, and the left splanchnic nerve was transected. In protocols requiring nerve stimulation, shielded bipolar stainless steel electrodes were applied to the distal end of the nerve, which was then stimulated with a digital stimulator (SEN-7203, Nihon Kohden, Japan) with a rectangular pulse (10 V and 1 ms in duration).

2.2. Dialysis technique

Dialysis probe construction was the same as that used in our previous dialysis experiments (Akiyama et al., 2003, 2004a,b). Each end of a dialysis fiber (0.32 mm OD, and 0.25 mm ID; PAN-DX 100,000 mol wt 100% cutoff, Asahi Chemical, Japan) was inserted into a polyethylene tube (25 cm length, 0.5 mm OD, and 0.2 mm ID; SP-8) and glued. The length of the dialysis fiber exposed was 3 mm. At a perfusion speed of 10 μl/min, *in vitro* recovery rates of ACh, norepinephrine (NE) and epinephrine (Epi) were (%): 3.21 ± 0.07, 2.68 ± 0.03, and 2.80 ± 0.03, respectively (number of dialysis probes: 3).

The left adrenal gland was gently lifted, and the dialysis probe was implanted in the medulla of the left adrenal gland along the long axis using a fine guiding needle. The dialysis probe was perfused with Ringer's solution or Ringer's solution containing pharmacological agents at a speed of 10 μl/min using a microinjection pump (CMA/100, Carnegie Medicin, Sweden). Ringer's solution consisted of (in mM) 147.0 NaCl, 4.0 KCl, 2.25 $CaCl_2$. All K_{Ca} channel antagonists tested were locally administered by perfusion through the dialysis probe after being dissolved in Ringer's solution. We started the protocols followed by a stabilization period of 3–4 h and sampled dialysate taking the dead space volume between the dialysis membrane and sample tube into account. Dialysate ACh and catecholamine concentrations were separately measured using each high-performance liquid chromatography with electrochemical detection as previously described (Akiyama et al., 2004a,b).

2.3. Experimental protocols

The experiment was performed based on the previous experiment showing that dialysate ACh and/or catecholamine responses were reproducible on repetition of the pharmacological or electrical stimulation (Akiyama et al., 2004a,b). At the end of the experiment, the rats were sacrificed with pentobarbital sodium, and the implant sites were examined. The dialysis probes were confirmed to have been implanted in the adrenal medulla, and no bleeding or necrosis was found macroscopically.

2.4. Protocol 1

We perfused the dialysis probe with Ringer's solution containing a cholinesterase inhibitor, neostigmine (10 μM) and investigated the effects of BK and SK channel antagonists on the nerve stimulation-induced responses of dialysate ACh and catecholamine concentration. The left splanchnic nerves were firstly electrically stimulated for 2 min at 2 Hz. Then, after a 30-min interval, nerves were subjected to a second stimulation for 2 min at 4 Hz. After these control stimulations, local administration of iberiotoxin (1 μM, $n = 7$), paxilline (100 μM, $n = 7$), apamin (10 μM, $n = 7$) or scyllatoxin (2 μM, $n = 7$) was started. Thirty minutes after local administration of K_{Ca} channel antagonists, nerves were stimulated for 2 min at 2 Hz. Next, after a 30-min interval, nerves were stimulated again for 2 min at 4 Hz. Phosphate buffer (pH 3.5, 4 μl) was transferred into each sample tube before dialysate sampling. Two dialysate samples were continuously collected per nerve stimulation: one before and one during stimulation. One sampling period was 2 min (1 sample volume = 20 μl). Half of the dialysate sample was used for the measurement of ACh, and the remaining half for the measurement of NE and Epi.

2.5. Protocol 2

We investigated the effects of K_{Ca} channel antagonists on the nerve stimulation-induced catecholamine release in the absence of neostigmine. Like in protocol 1, the left splanchnic nerves were stimulated before and 30 min after administration of iberiotoxin ($n = 7$), paxilline ($n = 7$), apamin ($n = 7$) or scyllatoxin ($n = 7$) and two dialysate samples were collected per nerve stimulation. The dialysate sample was used for the measurement of NE and Epi.

2.6. Protocol 3

We investigated the effects of K_{Ca} channel antagonists on exogenous ACh-induced catecholamine release. The dialysis probe was perfused with Ringer's solution. ACh (1 mM) was locally administered to the adrenal medulla through the dialysis probe for 1 min. After first administration of ACh, local administration of iberiotoxin (1 μM, $n = 7$), paxilline (100 μM, $n = 7$), apamin (10 μM, $n = 7$) or scyllatoxin (2 μM, $n = 7$) was started. Thirty minutes after local administration of K_{Ca} channel antagonists, ACh (1 mM) was locally administered again for 1 min. Phosphate buffer (pH 3.5, 2 μl) was transferred into each sample tube before dialysate sampling. Two dialysate samples were continuously collected per local administration of ACh: one before and one during administration. One sampling period was 1 min (1 sample volume = 10 μl). The dialysate sample was used for the measurement of NE and Epi.

2.7. Drugs

Drugs were mixed fresh for each experiment. Neostigmine methylsulfate (Shionogi, Japan), iberiotoxin (Peptide Institute, Japan), apamin (Peptide Institute) and scyllatoxin (Peptide Institute) were dissolved and diluted in Ringer's solution. Paxilline (Sigma Chemical, USA) was dissolved in DMSO and diluted in Ringer's solution. The final concentration of DMSO in the working solution was 0.5% (v/v).

2.8. Statistical methods

To examine the effects of nerve stimulation, local administration of ACh, and K_{Ca} channel antagonists, we analyzed heart rate and mean arterial pressure, basal dialysate NE and Epi content, and dialysate ACh, NE and Epi responses, by using one-way analysis of variance with repeated measures. When statistical significance was detected, the Newman–Keuls test was applied (Winer, 1971). Statistical significance was defined as $P < 0.05$. Values are presented as means ± SE.

3. Results

3.1. Changes in heart rate and mean arterial pressure

Local administration of neostigmine, K_{Ca} channel antagonists, and ACh through the dialysis probe did not change basal heart rate or mean arterial pressure. In protocol 1, nerve stimulation increased mean arterial pressure from 113 ± 3 mmHg in control to 131 ± 2 mmHg at 2 Hz ($n = 28$, $P < 0.05$) and 132 ± 2 mmHg at 4 Hz ($n = 28$, $P < 0.05$), and decreased heart rate from 436 ± 4 beats/min in control to 424 ± 4 beats/min at 2 Hz ($n = 28$, $P < 0.05$) and 420 ± 4 beats/min at 4 Hz ($n = 28$, $P < 0.05$). In protocol 2, nerve stimulation increased mean arterial pressure from 115 ± 4 mmHg in control to 129 ± 3 mmHg at 2 Hz ($n = 28$, $P < 0.05$) and 131 ± 3 mmHg at 4 Hz ($n = 28$, $P < 0.05$), and decreased heart rate from 423 ± 3 beats/min in control to 410 ± 4 beats/min at 2 Hz ($n = 28$, $P < 0.05$) and 404 ± 3 beats/min at 4 Hz ($n = 28$, $P < 0.05$). Heart rate and mean arterial pressure recovered to basal levels after nerve stimulation. After administration of K_{Ca} channel antagonists, nerve stimulation evoked the same responses of heart rate and mean arterial pressure.

Please cite this article in press as: Akiyama, T., et al., Role of Ca^{2+}-activated K^+ channels in catecholamine release from *in vivo* rat adrenal medulla. Neurochem. Int. (2009), doi:10.1016/j.neuint.2009.10.010

Table 1
Basal NE and Epi release before and after local administration of K_{Ca} channel antagonists.

	NE (nM)	Epi (nM)
Iberiotoxin ($n=21$)		
Before administration	4.8 ± 0.3	16.7 ± 1.0
After administration	5.0 ± 0.4	21.7 ± 1.6*
Paxilline ($n=21$)		
Before administration	4.7 ± 0.3	15.7 ± 1.1
After administration	4.8 ± 0.4	22.0 ± 1.9*
Apamin ($n=21$)		
Before administration	4.9 ± 0.4	17.1 ± 1.1
After administration	4.6 ± 0.5	21.2 ± 1.6*
Scyllatoxin ($n=21$)		
Before administration	4.9 ± 0.3	15.3 ± 0.7
After administration	5.1 ± 0.4	20.6 ± 0.9*

Values are means ± SE. n, no. of rats; NE, norepinephrine; Epi, epinephrine. *$P < 0.05$ vs. values before administration.

3.2. Basal ACh and catecholamine release

ACh could not be detected in dialysate before nerve stimulation even in the presence of neostigmine. In contrast, substantial amounts of NE and Epi were observed in dialysate before nerve stimulation or ACh administration. Local administration of neostigmine did not influence this basal catecholamine release. BK channel antagonists, iberiotoxin and paxilline did not change basal NE release but increased basal Epi release. Similarly, the SK channel antagonists, apamin and scyllatoxin did not change basal NE release, but increased basal Epi release (Table 1).

ACh was detected in dialysate only during nerve stimulation in the presence of neostigmine. Thus, we expressed this detected dialysate ACh concentration as an index of ACh release induced by nerve stimulation. In contrast, we subtracted basal dialysate NE and Epi content before nerve stimulation or ACh administration from those during stimulation or ACh administration, and expressed these subtracted values as indices of NE and Epi release induced by nerve stimulation or ACh administration.

3.3. Effects of K_{Ca} channel antagonists on the nerve stimulation-induced ACh and catecholamine release in the presence of neostigmine

Iberiotoxin enhanced the nerve stimulation-induced release of presynaptic ACh and postsynaptic catecholamine (Fig. 1A). ACh release increased from 4.5 ± 0.8 to 7.4 ± 0.7 nM at 2 Hz and from 9.4 ± 1.0 to 14.0 ± 1.0 nM at 4 Hz. NE release increased from 7 ± 0.5 to 32 ± 3 nM at 2 Hz and from 27 ± 3 to 74 ± 9 nM at 4 Hz. Epi release increased from 39 ± 5 to 78 ± 5 nM at 2 Hz, and from 105 ± 8 to 193 ± 15 nM at 4 Hz. Similarly, paxilline enhanced the nerve stimulation-induced release of ACh and catecholamine (Fig. 1B). ACh release increased from 4.1 ± 0.4 to 5.9 ± 0.5 nM at 2 Hz and from 9.4 ± 0.7 to 13.7 ± 0.9 nM at 4 Hz. NE release increased from 11 ± 2 to 26 ± 4 nM at 2 Hz, from 31 ± 5 to 58 ± 8 nM at 4 Hz. Epi release increased from 41 ± 7 to 77 ± 14 nM at 2 Hz and from 108 ± 14 to 195 ± 17 nM at 4 Hz.

Apamin had no effect on the nerve stimulation-induced release of ACh and NE, but enhanced the nerve stimulation-induced Epi release (Fig. 2A). Epi release increased from 45 ± 3 to 59 ± 4 nM at 2 Hz and from 108 ± 7 to 139 ± 17 nM at 4 Hz. Scyllatoxin had no effect on the nerve stimulation-induced release of ACh and NE either, but enhanced the nerve stimulation-induced Epi release (Fig. 2B). Epi release increased from 37 ± 4 to 50 ± 3 nM at 2 Hz and from 122 ± 5 to 152 ± 12 nM at 4 Hz.

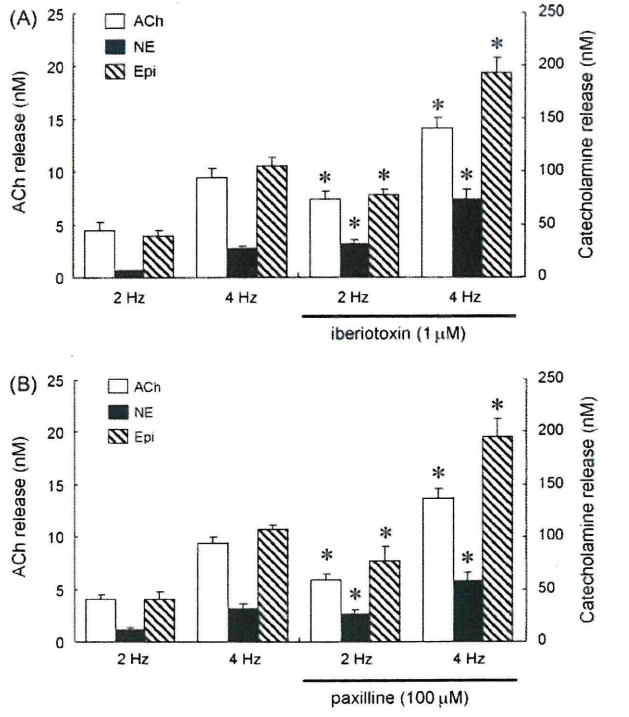

Fig. 1. Effects of BK channel antagonists on the nerve stimulation-induced release of acetylcholine (ACh), norepinephrine (NE) and epinephrine (Epi) in the presence of neostigmine (10 μM): iberiotoxin (A) and paxilline (B) enhanced the release of ACh, NE and Epi at 2 and 4 Hz. Values are means ± SE from seven rats. *$P < 0.05$ vs. ACh, NE or Epi release at the same frequency as before administration of BK channel antagonists.

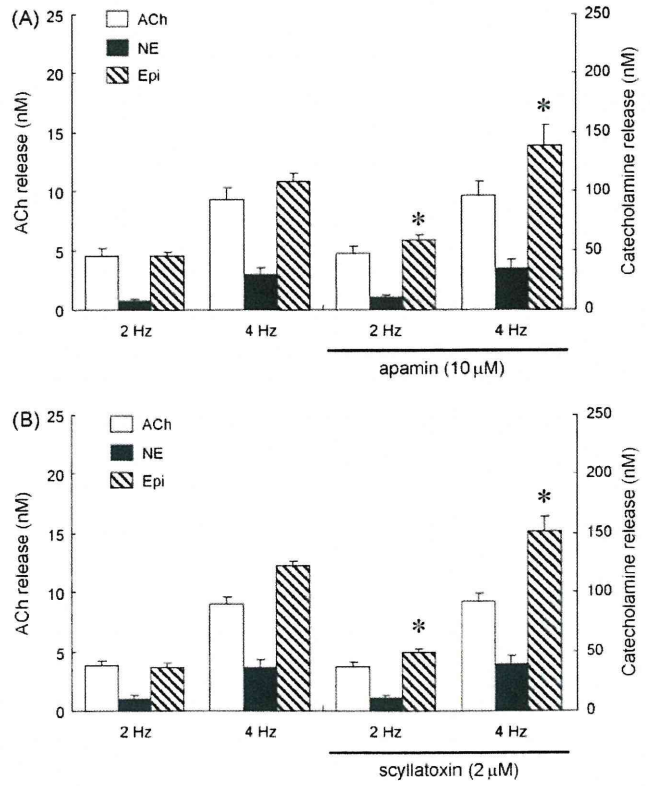

Fig. 2. Effects of SK channel antagonists on the nerve stimulation-induced release of ACh, NE and Epi in the presence of neostigmine (10 μM): apamin (A) and scyllatoxin (B) had no effect on the release of ACh or NE, but enhanced the Epi release at 2 and 4 Hz. Values are means ± SE from seven rats. *$P < 0.05$ vs. ACh, NE or Epi release at the same frequency as before administration of SK channel antagonists.

Please cite this article in press as: Akiyama, T., et al., Role of Ca^{2+}-activated K^+ channels in catecholamine release from *in vivo* rat adrenal medulla. Neurochem. Int. (2009), doi:10.1016/j.neuint.2009.10.010

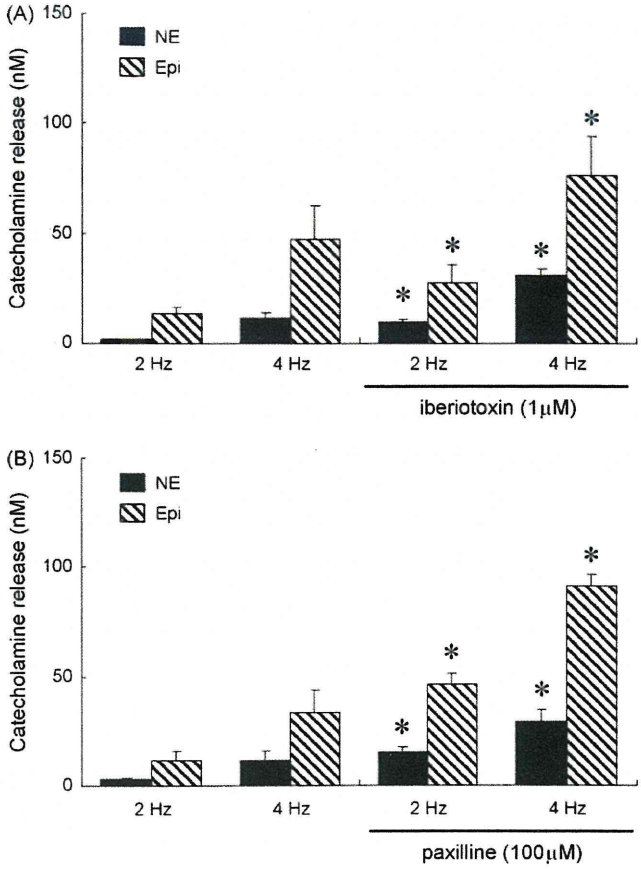

Fig. 3. Effects of BK channel antagonists on the nerve stimulation-induced release of NE and Epi in the absence of neostigmine: iberiotoxin (A) and paxilline (B) enhanced the release of NE and Epi at 2 and 4 Hz. Values are means ± SE from seven rats. *$P < 0.05$ vs. NE or Epi release at the same frequency as before administration of BK channel antagonists.

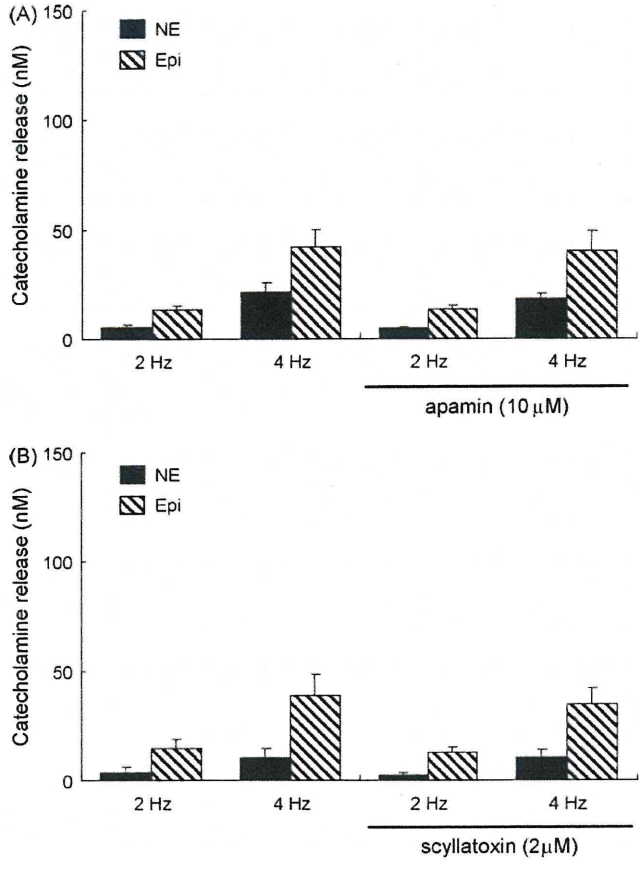

Fig. 4. Effects of SK channel antagonists on the nerve stimulation-induced release of NE and Epi in the absence of neostigmine: apamin (A) and scyllatoxin (B) had no effect on the release of NE or Epi at 2 or 4 Hz. Values are means ± SE from seven rats.

3.4. Effects of K_{Ca} channel antagonists on the nerve stimulation-induced catecholamine release in the absence of neostigmine

Iberiotoxin enhanced the nerve stimulation-induced catecholamine release at both 2 and 4 Hz (Fig. 3A). NE release increased from 2 ± 0.3 to 10 ± 2 nM at 2 Hz and from 12 ± 3 to 31 ± 3 nM at 4 Hz. Epi release increased from 13 ± 3 to 27 ± 9 nM at 2 Hz and from 47 ± 15 to 76 ± 18 nM at 4 Hz. Similarly, paxilline enhanced the nerve stimulation-induced catecholamine release (Fig. 3B). NE release increased from 3 ± 0.6 to 15 ± 2 nM at 2 Hz and from 12 ± 4 to 29 ± 5 nM at 4 Hz. Epi release increased from 12 ± 4 to 46 ± 5 nM at 2 Hz and from 34 ± 10 to 91 ± 6 nM at 4 Hz. Apamin and scyllatoxin had no effect on the nerve stimulation-induced catecholamine release at 2 or 4 Hz (Fig. 4A and B).

3.5. Effects of K_{Ca} channel antagonists on the exogenous ACh-induced catecholamine release

Iberiotoxin had no effect on the exogenous ACh-induced NE release, but enhanced the exogenous ACh-induced Epi release. Epi release increased from 108 ± 11 to 127 ± 10 nM (Fig. 5A). Similarly, paxilline had no effect on the exogenous ACh-induced NE release but enhanced the exogenous ACh-induced Epi release. Epi release increased from 93 ± 5 to 137 ± 13 nM (Fig. 5B). Apamin enhanced the exogenous ACh-induced catecholamine release (Fig. 6A). NE release increased from 37 ± 4 to 49 ± 4 nM and Epi release from 103 ± 8 to 122 ± 9 nM. Similarly scyllatoxin enhanced the exogenous ACh-induced catecholamine release (Fig. 6B). NE release increased from 32 ± 3 to 47 ± 3 nM and Epi release from 108 ± 6 to 140 ± 11 nM.

4. Discussion

4.1. Roles of K_{Ca} channels on splanchnic nerve endings in presynaptic ACh release

We found that, in the *in vivo* adrenal medulla, both iberiotoxin and paxilline enhanced the nerve stimulation-induced release of presynaptic ACh at 2 and 4 Hz by ~50% in the presence of neostigmine (Fig. 1). BK channels currents have been confirmed on cholinergic nerve endings including motor nerves in the neuromuscular junction (Flink and Atchison, 2003), presynaptic nerves in the chick ciliary ganglion (Sun et al., 1999) and tracheal parasympathetic nerves (Zhang et al., 1998). Activation of the K_{Ca} conductance is considered to limit Ca^{2+} entry through voltage-dependent Ca^{2+}channels, and subsequently reduce transmitter release (Meir et al., 1999). Our results strongly suggest that BK channels are present on the splanchnic nerve endings and involved in the control of ACh release. In the perfused cat adrenal gland, charybdotoxin, a BK channel antagonist, enhanced catecholamine release when transmural electrical stimulation was applied at low external Ca^{2+} concentrations, but not when exogenous ACh was administered (Montiel et al., 1995). In the perfused rat adrenal gland, charybdotoxin enhanced the release of Epi and NE induced by transmural electrical stimulation, but not the release induced by administration of ACh (Nagayama et al., 2000b). These indirect studies suggested that BK channels may be involved in the control

Please cite this article in press as: Akiyama, T., et al., Role of Ca^{2+}-activated K^+ channels in catecholamine release from *in vivo* rat adrenal medulla. Neurochem. Int. (2009), doi:10.1016/j.neuint.2009.10.010

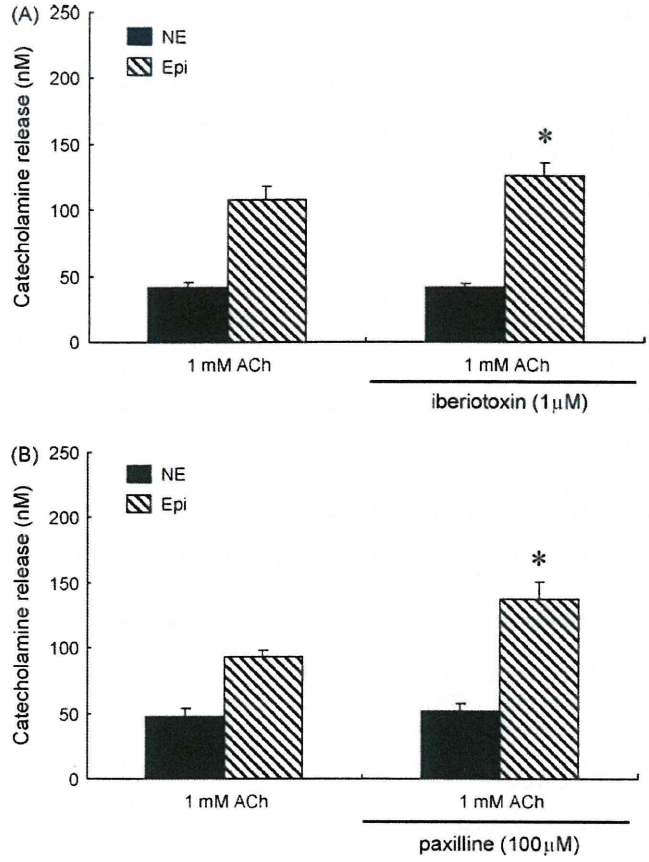

Fig. 5. Effects of BK channel antagonists on the exogenous ACh-induced release of NE and Epi: iberiotoxin (A) and paxilline (B) had no effect on NE release, but enhanced Epi release. Values are means ± SE from seven rats. *$P < 0.05$ vs. NE or Epi release before administration of BK channel antagonists.

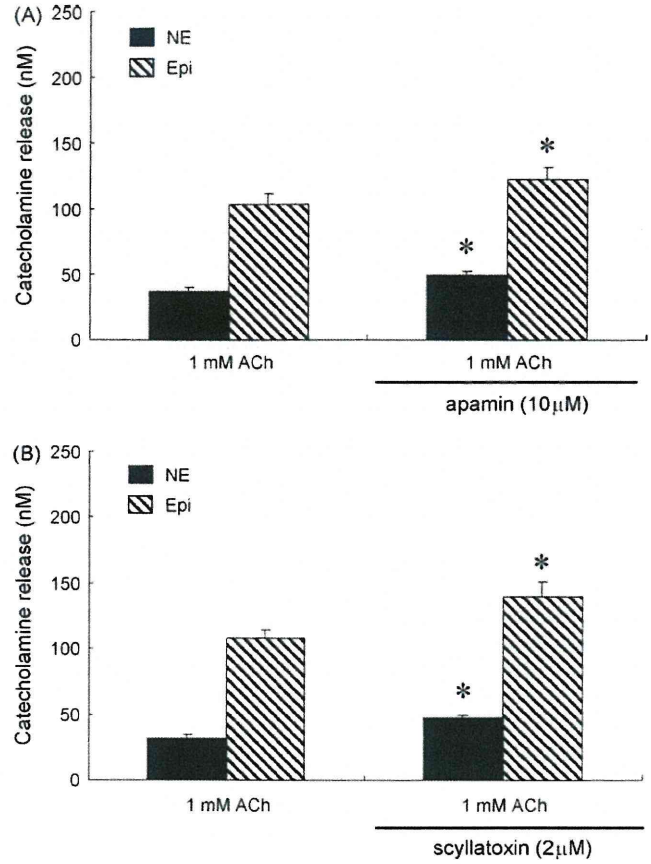

Fig. 6. Effects of SK channel antagonists on the exogenous ACh-induced release of NE and Epi: apamin (A) and scyllatoxin (B) enhanced the release of NE and Epi. Values are means ± SE from seven rats. *$P < 0.05$ vs. NE or Epi release before administration of SK channel antagonists.

of catecholamine release at the presynaptic site. But there has been no direct study investigating the effect of BK channel antagonists on ACh release from splanchnic nerve endings. This is the first direct study to demonstrate that BK channels are involved in the control of ACh release from splanchnic nerve endings. In the *in vivo* adrenal medulla, we observed a substantial enhancement of ACh release by BK channel antagonists at a frequency of 2 Hz with this degree of enhancement being similar to that at a frequency of 4 Hz (Fig. 1). BK channels on splanchnic nerve endings could be functional under physiological conditions. In our previous study, the nerve stimulation-induced catecholamine release was in large part cholinergic in the presence or absence of neostigmine (Akiyama et al., 2003). Thus, BK channels play an inhibitory role in the physiological catecholamine release from adrenal medulla by limiting presynaptic ACh release.

In contrast to BK channel antagonists, apamin and scyllatoxin had no effect on the nerve stimulation-induced ACh release at 2 or 4 Hz (Fig. 2). In perfused cat adrenal glands preloaded with [^{3}H]-choline, apamin did not modify the efflux of [^{3}H]-labeled compound evoked by transmural electrical stimulation (Montiel et al., 1995). SK channels seem to be absent on splanchnic nerve endings or play a minor role in the ACh release from splanchnic nerve endings.

4.2. Role of K_{Ca} channels on chromaffin cells in catecholamine release

Iberiotoxin and paxilline had no effect on the exogenous ACh-induced NE release, but enhanced exogenous ACh-induced Epi release (Fig. 5). Adrenal chromaffin cells are divided into two populations: NE- and Epi-storing cells (Coupland, 1984). While BK channels seem to be absent on NE-storing cells or play a minor role in the nerve stimulation-induced NE release, BK channels seem to be present on Epi-storing cells. It has been reported that BK channels present at rat chromaffin cells are activated by Ca^{2+} influx and contribute to the rapid termination of action potentials (Prakriya and Lingle, 1999), while iberiotoxin augments the nicotinic receptor-mediated catecholamine secretion from bovine adrenal chromaffin cells (Wada et al., 1995). The enhancement by BK channel antagonists of nerve stimulation-induced Epi release may be in part ascribed to their direct effects on Epi-storing cells. BK channels on Epi-storing cells may be involved in the control of nerve stimulation-induced Epi release. In perfused rat and cat adrenal glands, charybdotoxin, a BK channel antagonist, does not affect the exogenous ACh-induced catecholamine release (Montiel et al., 1995; Nagayama et al., 2000b). Our results of Epi release were inconsistent with these studies, possibly due to differences in the BK channel antagonists used and/or in methodology because charybdotoxin is pharmacologically less selective than iberiotoxin for BK channels (Garcia et al., 1991).

Both apamin and scyllatoxin enhanced the nerve stimulation-induced Epi release in the presence of neostigmine without changes in ACh release (Fig. 2), and the exogenous ACh-induced release of NE and Epi (Fig. 6). These results suggest that SK channels are present on both NE- and Epi-storing cells and that such enhancement is due to the direct effects of SK channel antagonists on chromaffin cells. Neither apamin nor scyllatoxin, however, had any effect on the nerve stimulation-induced NE release in the presence or absence of neostigmine, and the nerve

Please cite this article in press as: Akiyama, T., et al., Role of Ca^{2+}-activated K^+ channels in catecholamine release from *in vivo* rat adrenal medulla. Neurochem. Int. (2009), doi:10.1016/j.neuint.2009.10.010

stimulation-induced Epi release in the absence of neostigmine (Figs. 2 and 4). SK channels on chromaffin cells may play a minor role in the nerve stimulation-induced catecholamine release. It has been reported that SK channels on chromaffin cells are activated by muscarinic receptor stimulation (Nagayama et al., 2000a; Uceda et al., 1992). In our previous study of the same preparation, we demonstrated that muscarinic receptors are present on NE- and Epi-storing cells but play a minor role in the nerve stimulation-induced release of NE and Epi, and that cholinesterase inhibitor elicited muscarinic receptor-mediated Epi release when splanchnic nerve was stimulated (Akiyama et al., 2003). Therefore, SK channels on NE- and Epi-storing cells play an important role in the catecholamine release induced by activation of muscarinic or non-cholinergic receptors including PACAP receptor (Fukushima et al., 2002).

In the perfused rat adrenal gland, apamin enhanced NE release induced by transmural electrical stimulation and a nicotinic receptor agonist (Nagayama et al., 2000b). Therefore, SK channels on NE-storing cells could be activated by nicotinic as well as muscarinic receptors. But, our results of NE release induced by nerve stimulation were inconsistent with this study. In anesthetized dogs, scyllatoxin enhanced catecholamine release induced by a nicotinic receptor agonist but did not affect catecholamine release induced by splanchnic nerve stimulation (Nagayama et al., 1998). Thus, this inconsistency may be due to the difference in the method of nerve stimulation and SK channels on NE-storing cells may be activated by nicotinic receptors in the extrasynaptic region.

4.3. Roles of K_{Ca} channels in basal NE and Epi release

In the present study, substantial basal release of NE and Epi was observed in dialysate before nerve stimulation or ACh administration. Both BK and SK channel antagonists enhanced the basal Epi release but not the basal NE release. In our preparation, splanchnic nerves had been transected before control sampling and basal catecholamine release was not enhanced by a cholinesterase inhibitor, neostigmine. Furthermore, using the same preparation we demonstrated that basal catecholamine release is resistant to not only cholinergic antagonists, but also N-, P/Q-, and L-type Ca^{2+} channel antagonists (Akiyama et al., 2004b). Basal catecholamine release seems to be non-cholinergic and independent of Ca^{2+} influx through voltage-dependent Ca^{2+} channels. Ca^{2+} release from intracellular Ca^{2+} stores may be involved in this basal catecholamine release. It has been suggested in chromaffin cells that K_{Ca} channels on the cell surface are activated by Ca^{2+} release from intracellular Ca^{2+} stores (Ohta et al., 1998). On Epi-storing cells, BK and SK channels may play a role in the Epi release induced by Ca^{2+} release from intracellular Ca^{2+} stores.

4.4. Methodological considerations

Because previous results suggested that distribution across the dialysis membrane is required (Akiyama et al., 2003, 2004a), we used the K_{Ca} channel antagonists at a concentration 10 times higher than that required for complete channel blockade in experimental settings *in vitro*. Then, we tested two different types of selective BK and SK channel antagonists in the present study because higher concentrations of K_{Ca} channel antagonists might induce other pharmacological effects.

Cholinesterase inhibitor was necessary to monitor endogenous ACh even during the splanchnic nerve stimulation because released ACh is rapidly degraded by acetylcholinesterase before reaching the dialysis fiber. Then, we examined the effects of K_{Ca} channel antagonists in the presence or absence of neostigmine because neostigmine may influence the effects of K_{Ca} channel antagonists. Local administration of neostigmine enhanced the nerve stimulation-induced catecholamine release to about 2-fold before and after administration of K_{Ca} channel antagonists (Figs. 1 and 3). This enhancement could be due to the elevation of synaptic ACh levels by inhibition of acetylcholinesterase.

5. Conclusion

We applied dialysis technique to the adrenal medulla of anesthetized rats and investigated the effects of K_{Ca} channel antagonists on the presynaptic ACh release from splanchnic nerve endings and the postsynaptic catecholamine release from chromaffin cells. BK channels on presynaptic splanchnic nerve endings play an inhibitory role in the physiological catecholamine release from adrenal medulla by limiting presynaptic ACh release while SK channels do not. BK channels on Epi-storing cells may play an inhibitory role in the nerve stimulation-induced Epi release. SK channels are present on NE- and Epi-storing cells, but play a minor role in the nerve stimulation-induced catecholamine release.

Acknowledgment

This work was supported by a Grant-in-Aid for scientific research (No. 19591829) from the Ministry of Education, Culture, Sports, Science and Technology.

References

Akiyama, T., Yamazaki, T., Mori, H., Sunagawa, K., 2003. Inhibition of cholinesterase elicits muscarinic receptor-mediated synaptic transmission in the rat adrenal medulla. Auton. Neurosci. 107, 65–73.
Akiyama, T., Yamazaki, T., Mori, H., Sunagawa, K., 2004a. Simultaneous monitoring of acetylcholine and catecholamine release in the in vivo rat adrenal medulla. Neurochem. Int. 44, 497–503.
Akiyama, T., Yamazaki, T., Mori, H., Sunagawa, K., 2004b. Effects of Ca^{2+} channel antagonists on acetylcholine and catecholamine releases in the in vivo rat adrenal medulla. Am. J. Physiol. 287, R161–R166.
Auguste, P., Hugues, M., Gravé, B., Gesquière, J.C., Maes, P., Tartar, A., Romey, G., Schweitz, H., Lazdunski, M., 1990. Leiurotoxin I (scyllatoxin), a peptide ligand for Ca^{2+}-activated K^+ channels. J. Biol. Chem. 265, 4753–4759.
Blatz, A., Magleby, K.L., 1986. Single apamin-blocked Ca-activated K^+ channels of small conductance in cultured rat skeletal muscle. Nature 323, 718–720.
Blatz, A., Magleby, K.L., 1987. Calcium-activated potassium channels. Trends. Neurosci. 10, 463–467.
Candia, S., Garcia, M.L., Latorre, R., 1992. Mode of action of iberiotoxin, a potent blocker of the large conductance Ca^{2+}-activated K^+ channel. Biophys. J. 63, 583–590.
Coupland, R.E., 1965. The Natural History of the Chromaffin Cell. Longmans, London.
Coupland, R.E., 1984. Ultrastructural features of the mammalian adrenal medulla. In: Motta, P.M. (Ed.), Ultrastructure of Endocrine Cells and Tissues. Nijhoff, Boston, MA, pp. 168–179.
Flink, M.T., Atchison, W.D., 2003. Iberiotoxin-induced block of Ca^{2+}-activated K^+ channels induces dihydropyridine sensitivity of ACh release from mammalian motor nerve terminals. J. Pharmacol. Exp. Ther. 305, 646–652.
Fukushima, Y., Nagayama, T., Hikichi, H., Mizukami, K., Yoshida, M., Suzuki-Kusaba, M., Hisa, H., Kimura, T., Satoh, S., 2002. Role of K^+ channels in the PACAP-induced catecholamine secretion from the rat adrenal gland. Eur. J. Pharmacol. 437, 69–72.
García, A.G., García-De-Diego, A.M., Gandía, L., Borges, R., García-Sancho, J., 2006. Calcium signaling and exocytosis in adrenal chromaffin cells. Physiol. Rev. 86, 1093–1131.
Garcia, M.L., Galvez, A., Garcia-Calvo, M., King, V.F., Vazquez, J., Kaczorowski, G.J., 1991. Use of toxins to study potassium channels. J. Bioenerg. Biomembr. 23, 615–646.
Kanus, H.G., McManus, O.B., Lee, S.H., Schmalhofer, W.A., Galcia-Calvo, M., Helms, L.M., Sanchez, M., Giangiacomo, K., Reuben, J.P., Smith, A.B., 1994. Tremorgenic indole alkaloids potently inhibit smooth muscle high-conductance calcium-activated potassium channels. Biochemistry 33, 5819–5828.
Meir, A., Ginsburg, S., Butkevich, A., Kachalsky, S.G., Kaiserman, I., Ahdut, R., Demirgoren, S., Rahamimoff, R., 1999. Ion channels in presynaptic nerve terminals and control of transmitter release. Physiol. Rev. 79, 1019–1088.
Montiel, C., López, M.G., Sánchez-García, P., Maroto, R., Zapater, P., García, A.G., 1995. Contribution of SK and BK channels in the control of catecholamine release by electrical stimulation of the cat adrenal gland. J. Physiol. 486, 427–437.

Please cite this article in press as: Akiyama, T., et al., Role of Ca^{2+}-activated K^+ channels in catecholamine release from *in vivo* rat adrenal medulla. Neurochem. Int. (2009), doi:10.1016/j.neuint.2009.10.010

Nagayama, T., Fukushima, Y., Hikichi, H., Yoshida, M., Suzuki-Kusaba, M., Hisa, H., Kimura, T., Satoh, S., 2000a. Interaction of SK_{Ca} channels and L-type Ca^{2+} channels in catecholamine secretion in the rat adrenal gland. Am. J. Physiol. 279, R1731–R1736.

Nagayama, T., Fukushima, Y., Yoshida, M., Suzuki-Kusaba, M., Hisa, H., Kimura, T., Satoh, S., 2000b. Role of potassium channels in catecholamine secretion in the rat adrenal gland. Am. J. Physiol. 279, R448–R454.

Nagayama, T., Masada, K., Yoshida, M., Suzuki-Kusaba, M., Hisa, H., Kimura, T., Satoh, S., 1998. Role of K^+ channels in adrenal catecholamine secretion in anesthetized dogs. Am. J. Physiol. 274, R1125–R1130.

Ohta, T., Ito, S., Nakazato, Y., 1998. Ca^{2+}-dependent K^+ currents induced by muscarinic receptor activation in guinea pig adrenal chromaffin cells. J. Neurochem. 70, 1280–1288.

Prakriya, M., Lingle, C.J., 1999. BK channel activation by brief deporalizations requires Ca^{2+} influx through L- and Q-type Ca^{2+} channels in rat chromaffin cells. J. Neurophysiol. 81, 2267–2278.

Sun, X.P., Schlichter, L.C., Stanley, E.F., 1999. Single-channel properties of BK-type calcium-activated potassium channels at a cholinergic presynaptic nerve terminal. J. Physiol. 518, 639–651.

Uceda, G., Artalejo, A.R., López, M.G., Abad, F., Neher, E., García, A.G., 1992. Ca^{2+}-activated K^+ channels modulate muscarinic secretion in cat chromaffin cells. J. Physiol. 454, 213–230.

Wada, A., Urabe, M., Yuhi, T., Yamamoto, R., Yanagita, T., Niina, H., Kobayashi, H., 1995. Large- and small-conductance Ca^{2+}-activated K^+ channels: their role in the nicotinic receptor-mediated catecholamine secretion in bovine adrenal medulla. Naunyn Schmiedeberg's Arch. Pharmacol. 352, 545–549.

Winer, B.J., 1971. Statistical Principles in Experimental Design, 2nd ed. McGraw-Hill, New York.

Zhang, X.Y., Zhu, F.X., Robinson, N.E., 1998. Role of cAMP and neuronal K^+ channels on α_2-AR-induced inhibition of ACh release in equine trachea. Am. J. Physiol. 274, L827–L832.

Please cite this article in press as: Akiyama, T., et al., Role of Ca^{2+}-activated K^+ channels in catecholamine release from *in vivo* rat adrenal medulla. Neurochem. Int. (2009), doi:10.1016/j.neuint.2009.10.010

Autonomic Neuroscience: Basic and Clinical 152 (2010) 115–118

Contents lists available at ScienceDirect

Autonomic Neuroscience: Basic and Clinical

journal homepage: www.elsevier.com/locate/autneu

Short communication

In vivo direct monitoring of interstitial norepinephrine levels at the sinoatrial node

Shuji Shimizu [a,c,d,*], Tsuyoshi Akiyama [b], Toru Kawada [a], Toshiaki Shishido [a], Masaki Mizuno [a], Atsunori Kamiya [a], Toji Yamazaki [b], Shunji Sano [c], Masaru Sugimachi [a]

[a] Department of Cardiovascular Dynamics, Advanced Medical Engineering Center, National Cardiovascular Center Research Institute, Osaka, Japan
[b] Department of Cardiac Physiology, National Cardiovascular Center Research Institute, Osaka, Japan
[c] Department of Cardiovascular Surgery, Okayama University Graduate School of Medicine, Dentistry and Pharmaceutical Sciences, Okayama, Japan
[d] Japan Association for the Advancement of Medical Equipment, Tokyo, Japan

ARTICLE INFO

Article history:
Received 1 June 2009
Received in revised form 12 August 2009
Accepted 27 August 2009

Keywords:
Heart rate
Sympathetic nerve terminal activity
Norepinephrine
Sinoatrial node
Microdialysis
Desipramine

ABSTRACT

We assessed in vivo interstitial norepinephrine (NE) levels at the sinoatrial node in rabbits, using microdialysis technique. A dialysis probe was implanted adjacent to the sinoatrial node of an anesthetized rabbit and dialysate was sampled during sympathetic nerve stimulation. Atrial dialysate NE concentration correlated well with heart rate. Desipramine significantly increased dialysate NE concentrations both before and during sympathetic nerve stimulation compared with the absence of desipramine. However, desipramine did not affect the relation between heart rate and dialysate NE concentration. These results suggest that atrial dialysate NE level reflects the relative change of NE concentration in the synaptic cleft. Microdialysis is a powerful tool to assess in vivo interstitial NE levels at the sinoatrial node.

1. Introduction

Heart rate is determined by the frequency of depolarization of sinoatrial (SA) nodal cell during sinus rhythm. The SA node is innervated by sympathetic nerve fibers. These sympathetic nerves, together with parasympathetic nerves, play an important role in the regulation of SA node pacemaker activities. Direct measurement of electrical axonal activity of efferent cardiac sympathetic nerve (Kawada et al., 2004) and indirect measurement of norepinephrine (NE) spillover from plasma NE concentration in the coronary sinus (Meredith et al., 1993) have been used as indices of sympathetic nerve terminal activity on the effector, i.e. sinoatrial node. However, due to the heterogeneity of sympathetic innervation in the heart, quantitative assessment of sympathetic nerve terminal activities on the SA node is essential for better understanding of the sympathetic control of heart rate.

Recently we have developed a microdialysis technique that allows direct monitoring of acetylcholine release into the SA node (Shimizu et al., 2009). In the present study, we monitored interstitial NE levels in the right atrial myocardium adjacent to the SA node using the microdialysis technique and investigated the relation between interstitial NE levels and heart rate in response to sympathetic nerve stimulation. This study may prove the usefulness of microdialysis in assessing the relative change of sympathetic nerve terminal activity on the SA mode.

2. Materials and methods

2.1. Surgical preparation

Animal care was provided in accordance with the *Guiding Principles for the Care and Use of Animals in the Field of Physiological Sciences* approved by the Physiological Society of Japan. All protocols were approved by the Animal Subject Committee of the National Cardiovascular Center. Fourteen Japanese white rabbits weighing 2.4 to 2.8 kg were used in this study. Anesthesia was initiated by an intravenous injection of pentobarbital sodium (50 mg/kg) via the marginal ear vein, and then maintained at an appropriate level by continuous intravenous infusion of α-chloralose and urethane (16 mg/kg/h and 100 mg/kg/h) through a catheter inserted into the femoral vein. The animals were intubated and ventilated mechanically with room air mixed with oxygen. Systemic arterial pressure was monitored by a catheter inserted into the femoral artery. Esophageal temperature, which was measured by a thermometer (CTM-303, Terumo, Japan), was maintained between 38 and 39 °C using a heating pad. Bilateral vagal nerves were exposed through a midline cervical incision and sectioned at the neck.

With the animal in supine position, a full median sternotomy was performed to expose the heart. The right cardiac sympathetic nerve

* Corresponding author. Department of Cardiovascular Dynamics, Advanced Medical Engineering Center, National Cardiovascular Center Research Institute, 5-7-1, Fujishiro-dai, Suita, Osaka, 565-8565, Japan. Tel.: +81 6 6833 5012; fax: +81 6 6835 5403.
E-mail address: shujismz@ri.ncvc.go.jp (S. Shimizu).

1566-0702/$ – see front matter © 2009 Elsevier B.V. All rights reserved.
doi:10.1016/j.autneu.2009.08.017

was exposed through the sternotomy and sectioned intrathoracically. A pair of bipolar stainless steel electrodes was attached to the efferent side of the right cardiac sympathetic nerve. The nerve and electrode were immobilized using a quick-dry silicone gel (Kwik-Cast and Kwik-Sil, World Precision Instruments, Inc., FL, USA). When sympathetic stimulation was required, the efferent sympathetic nerve was stimulated by a digital stimulator (SEN-7203, Nihon Kohden, Japan), at a pulse duration of 1 ms and an amplitude of 5 V. Three stainless electrodes were attached around the incision of sternotomy for the body surface electrocardiogram. The heart rate was determined from the electrocardiogram using a cardiotachometer. Heparin sodium (100 IU/kg) was administered intravenously to prevent blood coagulation. A dialysis probe was implanted and dialysis was conducted as described in *Dialysis Technique* below. At the end of the experiment, the animal was euthanized with an overdose injection of pentobarbital sodium. In the postmortem examination, the right atrial wall was resected with dialysis fiber. We observed the inside of atrial wall macroscopically and confirmed that the dialysis membrane was not exposed to right atrial lumen.

2.2. Dialysis technique

The materials and properties of the dialysis probe have been described previously. (Akiyama et al., 1991; Shimizu et al., 2009) A dialysis fiber of semipermeable membrane (4 mm length, 310 μm outer diameter, 200 μm inner diameter; PAN-1200, 50,000 molecular weight cutoff; Asahi Chemical, Tokyo, Japan) was attached at both ends to polyethylene tubes (25 cm length, 500 μm outer diameter, 200 μm inner diameter). A fine guiding needle (30 mm length, 510 μm outer diameter, 250 μm inner diameter) with a stainless steel rod (5 mm length, 250 μm outer diameter) was used for the implantation of the dialysis probe. A dialysis probe was implanted into the right atrial myocardium near the junction between the superior vena cava and the right atrium. After implantation, the dialysis probe was perfused with Ringer's solution (NaCl 147 mM, KCl 4 mM, $CaCl_2$ 3 mM) at a speed of 2 μl/min, using a microinjection pump (CMA/102, Carnegie Medicin, Sweden). Experimental protocols were started 120 min after implantation of the dialysis probe. We took account of the dead space between the dialysis membrane and the sample tube at the start of each dialysate sampling. Four-μl phosphate buffer (pH 3.5) was transferred into each sample tube before dialysate sampling. Dialysate sampling periods were set at 10 min (1 sample volume = 20 μl). Dialysate NE concentration was analyzed by high performance liquid chromatography (Akiyama et al., 1991).

2.3. Experimental protocols

2.3.1. Protocol 1

To examine whether atrial interstitial NE level reflects NE release from cardiac sympathetic nerve endings, we investigated the effect of sympathetic nerve stimulation on dialysate NE concentration and analyzed the relationship between the dialysate NE concentrations and heart rate ($n = 7$). We sampled control dialysate after transecting the right sympathetic nerve. Then we stimulated the right sympathetic nerve for 10 min each at frequencies of 2, 5 and 10 Hz, and collected the dialysate during each stimulation. There was a 30-min interval between the different stimulation frequencies. Twenty min after sympathetic nerve stimulation, we sampled the dialysate again to check for recovery of NE level.

2.3.2. Protocol 2

Most of the released NE is removed by neuronal uptake mechanism in the heart (Goldstein et al., 1988). To examine whether an increase in atrial interstitial NE level reflects the increase in synaptic NE levels associated with inhibition of neuronal uptake, we investigated the effects of sympathetic nerve stimulation on dialysate NE concentration in the presence of neuronal uptake inhibition and analyzed the relationship between dialysate NE concentration and heart rate ($n = 7$). After intravenous administration of a neuronal uptake inhibitor, desipramine (1.0 mg/kg), we stimulated the right sympathetic nerve and sampled the dialysate in a similar fashion as in Protocol 1.

2.4. Statistical analysis

All data are presented as means ± SE. Heart rate and dialysate NE concentrations (logarithmic transformation) in response to sympathetic stimulation were compared between the absence and presence of desipramine by two-way analysis of variance (ANOVA). If there was not a significant interaction between desipramine and stimulation effects, heart rate and dialysate NE concentrations (logarithmic transformation) in response to sympathetic stimulation were compared using Dunnett's test. After logarithmic transformation of dialysate NE concentration, a linear regression analysis was performed to examine the relation between dialysate NE concentration and heart rate. The differences in slope and intercept between two regression lines were examined. (Glantz, 2005) Differences were considered significant at $P < 0.05$.

3. Results

In Protocol 1 (stimulation alone), right cardiac sympathetic nerve stimulation significantly increased heart rate from 260 ± 8 bpm in the pre-stimulation control to 298 ± 11 bpm during stimulation at 2 Hz ($P < 0.01$ vs. control), 319 ± 10 bpm at 5 Hz ($P < 0.01$ vs. control) and 318 ± 11 bpm at 10 Hz ($P < 0.01$ vs. control) (ANOVA, $P < 0.001$). Heart rate recovered to 261 ± 9 bpm 20 min after stimulation. Right cardiac sympathetic nerve stimulation significantly increased dialysate NE concentration from 0.4 ± 0.1 nM in the pre-stimulation control to 1.0 ± 0.1 nM during stimulation at 2 Hz ($P < 0.01$ vs. control), 2.2 ± 0.5 nM at 5 Hz ($P < 0.01$ vs. control) and 2.9 ± 0.9 nM at 10 Hz ($P < 0.01$ vs. control) (ANOVA, $P < 0.001$). Dialysate NE concentration recovered to the pre-stimulation level 20 min after stimulation (0.6 ± 0.1 nM) (Fig. 1).

In Protocol 2 (desipramine + stimulation), intravenous administration of desipramine significantly increased baseline heart rate (295 ± 11 vs. 263 ± 11 bpm, $P < 0.01$, paired t test) and baseline dialysate NE concentration (1.5 ± 0.2 vs. 0.8 ± 0.2 nM, $P < 0.01$, paired t test) compared

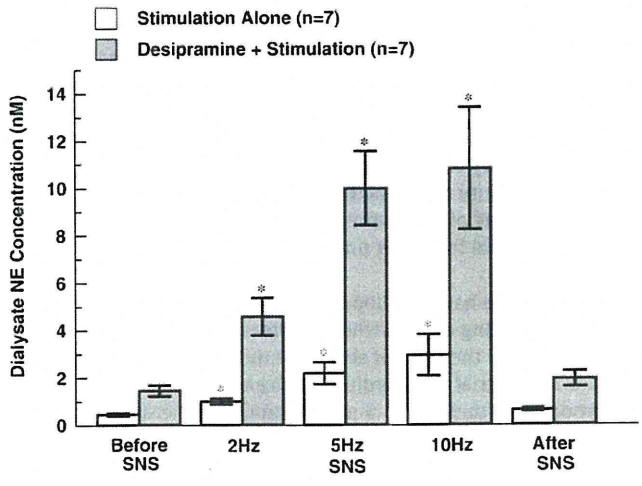

Fig. 1. Dialysate NE concentrations of controls and during electrical stimulation of right cardiac sympathetic nerve at different frequencies. The two-way analysis of variance (ANOVA) revealed the significant effect of sympathetic nerve stimulation on dialysate NE concentration ($P < 0.001$) and the significant difference in dialysate NE concentration ($P < 0.001$) between the absence and presence of desipramine. The interaction between desipramine and stimulation effects was not significant. Values are means ± SE; NE: norepinephrine; SNS: electrical sympathetic nerve stimulation; *n*: number of rabbits; *: $P < 0.01$ vs. the pre-stimulation control by Dunnett's test.

to Protocol 1. Right cardiac sympathetic nerve stimulation significantly increased heart rate from 295 ± 11 bpm in the pre-stimulation control to 349 ± 9 bpm during stimulation at 2 Hz ($P<0.01$ vs. control), 361 ± 8 bpm at 5 Hz ($P<0.01$ vs. control) and 351 ± 9 bpm at 10 Hz ($P<0.01$ vs. control) (ANOVA, $P<0.001$). Heart rate recovered to 295 ± 13 bpm 20 min after stimulation. Right sympathetic nerve stimulation also increased dialysate NE concentration from 1.5 ± 0.2 nM in the pre-stimulation control to 4.6 ± 0.8 nM during stimulation at 2 Hz ($P<0.01$ vs. control), 10.0 ± 1.6 nM at 5 Hz ($P<0.01$ vs. control) and 10.8 ± 2.6 nM at 10 Hz ($P<0.01$ vs. control) (ANOVA, $P<0.001$). Dialysate NE concentration recovered to the pre-stimulation level 20 min after stimulation (1.9 ± 0.3 nM) (Fig. 1). Heart rate and dialysate NE concentrations in Protocol 2 (desipramine + stimulation) were significantly higher than those in Protocol 1 (stimulation alone) (ANOVA, $P<0.001$). The interaction between desipramine and stimulation effects was not significant.

The relation between heart rate and dialysate NE concentration is shown in Fig. 2. Dialysate NE concentration correlated well with heart rate in both Protocols 1 and 2 (Protocol 1: $HR = 290 + 87 \times \log[NE(nM)]$, $R^2 = 0.71$; Protocol 2: $HR = 283 + 74 \times \log[NE(nM)]$, $R^2 = 0.70$) There was no significant difference in the intercept or slope between the two regression lines obtained from Protocols 1 and 2. (Glantz, 2005)

4. Discussion

We were able to monitor in vivo interstitial NE levels at the SA node using microdialysis technique. A neuronal uptake inhibitor, desipramine, significantly increased dialysate NE concentration in the right atrial myocardium. However, desipramine scarcely affected the relation between interstitial NE levels and heart rate.

4.1. Characteristics of dialysate NE concentration in right atrial myocardium

Dialysate NE concentration in the right atrial myocardium increased in response to electrical stimulation of the right cardiac sympathetic nerve and decreased to the pre-stimulation level after stimulation. These results indicate that atrial dialysate NE concentration reflects NE release from cardiac sympathetic nerve endings innervating the right atrium. Furthermore, a semi-log plot demonstrated a linear relationship between the right atrial dialysate NE concentration and heart rate. Judging from this relation, a 10-fold increase in dialysate NE concentration corresponds to an increase in heart rate of 87 bpm. The relative changes in NE release monitored by microdialysis correlate well with the frequency in depolarization of the SA nodal cell. Thus, we consider that dialysate NE concentration does reflect the relative changes in synaptic NE level. The relation between exogenous NE concentration and heart rate has been investigated in the isolated rabbit's atria (Toda, 1969). However, there is no report of a direct method to assess the endogenous NE release into the SA node. Microdialysis enables the monitoring of endogenous NE release into the SA node.

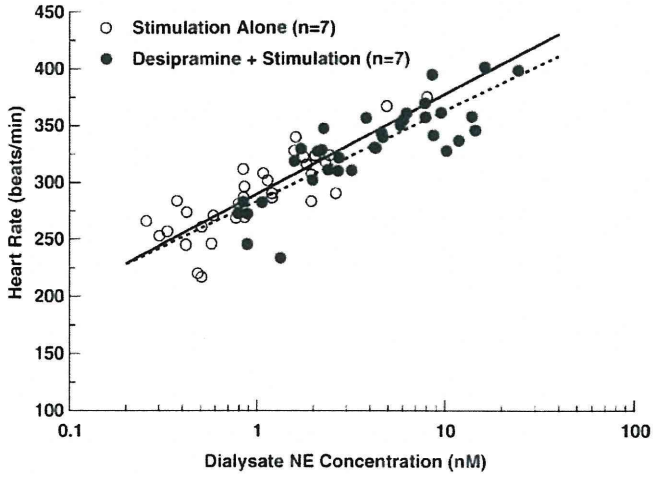

Fig. 2. Relation between dialysate NE concentration (logarithmic scale) and heart rate. Dialysate NE concentration in the right atrial myocardium correlates well with heart rate. Solid line: regression line fitting 35 data points obtained from Protocol 1 (stimulation alone) ($R^2 = 0.71$); dotted line: regression line fitting 35 data points obtained from Protocol 2 (desipramine + stimulation) ($R^2 = 0.70$). NE: norepinephrine.

4.2. Effect of neuronal uptake on dialysate NE concentration

In the presence of desipramine, a neuronal uptake inhibitor, dialysate NE concentration also increased in response to sympathetic nerve stimulation and decreased to the pre-stimulation levels after stimulation. However, dialysate NE concentrations were 3.1–4.6 times higher than the corresponding values in the absence of desipramine. These results are consistent with earlier experimental studies demonstrating that a large part of released NE is removed by neuronal uptake (Goldstein et al., 1988). In the present study, we were able to monitor the change in neuronal NE uptake function induced by desipramine using microdialysis technique.

Linked with the increase in dialysate NE concentrations in the presence of desipramine, heart rates were 33–51 bpm higher than the corresponding values in the absence of desipramine. Thus, desipramine does not alter the relation between dialysate NE concentration and heart rate. The intercept and the slope of regression line also did not differ significantly in the presence and absence of desipramine. These results indicate that neuronal uptake removes effective NE from the synaptic cleft without affecting the sensitivity of the SA nodal cell, and that neuronal NE uptake function plays an important role in the regulation of heart rate. The increase in synaptic NE concentration induced by inhibition of neuronal uptake affects the frequency of depolarization of the SA nodal cell.

Endoh (1975) reported that desipramine shifted the dose–response curve for exogenous NE to the lower NE levels. Since desipramine suppresses the neuronal uptake of both endogenous and exogenous NE, the increase in effective NE on the sinoatrial node may yield this apparent shift in the dose–response curve. Our results suggest that desipramine-inhibited neuronal uptake scarcely affects the relation between synaptic NE concentration and heart rate. Therefore, microdialysis may be a powerful tool to assess the change of synaptic NE concentration in the SA node.

4.3. Limitation

There were several limitations in the present study. First, since we did not section the left cardiac sympathetic nerve, the influence of left sympathetic nerve on the dialysate NE concentration cannot be excluded. Therefore, intravenous administration of desipramine could inhibit neuronal NE uptake at the left sympathetic nerve endings and increase dialysate NE concentration. Second, desipramine may affect the dynamic response of heart rate to sympathetic activation. We have already reported that desipramine decreases the natural frequency of the transfer function from sympathetic nerve activity to heart rate (Kawada et al., 2004). However, cardiac microdialysis using shorter dialysis fiber requires 10-min sampling time to detect changes in myocardial interstitial NE levels. Therefore, we were not able to investigate the dynamic response of heart rate to sympathetic activation in this study.

4.4. Conclusion

We were able to monitor endogenous NE release into the SA node and detect the changes in neuronal uptake function using microdialysis technique. Neuronal NE uptake together with NE release functions play

an important role in the regulation of synaptic NE concentration in the SA node. Microdialysis is a powerful tool to assess the changes of synaptic NE concentration in the SA node.

Acknowledgements

This study was supported by Health and Labor Sciences Research Grants (H18-nano-Ippan-003, H19-nano-Ippan-009, H20-katsudo-Shitei-007 and H21-nano-Ippan-005) from the Ministry of Health, Labor and Welfare of Japan, by Grants-in-Aid for Scientific Research (No. 20390462) from the Ministry of Education, Culture, Sports, Science and Technology in Japan and by the Industrial Technology Research Grant Program from New Energy and Industrial Technology Development Organization (NEDO) of Japan.

References

Akiyama, T., Yamazaki, T., Ninomiya, I., 1991. In vivo monitoring of myocardial interstitial norepinephrine by dialysis technique. Am. J. Physiol. 261, H1643–H1647.

Endoh, M., 1975. Effects of dopamine on sinus rate and ventricular contractile force of the dog heart in vitro and in vivo. Br. J. Pharmacol. 55, 475–486.

Glantz, S.A., 2005. Primer of Biostatistics, 6th ed. McGraw-Hill, New York.

Goldstein, D.S., Brush Jr., J.E., Eisenhofer, G., Stull, R., Esler, M., 1988. In vivo measurement of neuronal uptake of norepinephrine in the human heart. Circulation 78, 41–48.

Kawada, T., Miyamoto, T., Uemura, K., Kashihara, K., Kamiya, A., Sugimachi, M., Sunagawa, K., 2004. Effects of neuronal norepinephrine uptake blockade on baroreflex neural and peripheral arc transfer characteristics. Am. J. Physiol. Regul. Integr. Comp. Physiol. 286, R1110–R1120.

Meredith, I.T., Eisenhofer, G., Lambert, G.W., Dewar, E.M., Jennings, G.L., Esler, M.D., 1993. Cardiac sympathetic nervous activity in congestive heart failure. Evidence for increased neuronal norepinephrine release and preserved neuronal uptake. Circulation 88, 136–145.

Shimizu, S., Akiyama, T., Kawada, T., Shishido, T., Yamazaki, T., Kamiya, A., Mizuno, M., Sano, S., Sugimachi, M., 2009. In vivo direct monitoring of vagal acetylcholine release to the sinoatrial node. Auton. Neurosci. 148, 44–49.

Toda, N., 1969. Interactions of ouabain and noradrenaline in isolated rabbit's atria. Br. J. Pharmacol. 36, 393–408.

32nd Annual International Conference of the IEEE EMBS
Buenos Aires, Argentina, August 31 - September 4, 2010

Development of artificial bionic baroreflex system

Kenji Sunagawa, *Senior Member, IEEE* and Masaru Sugimachi, *Member, IEEE*

Abstract—**The baroreflex system is the fastest mechanism in the body to regulate arterial pressure. Because the neural system (i.e., autonomic nervous system) mediates the baroreflex and the system operates under the closed-loop condition, the quantitative dynamic characteristics of the baroreflex system remained unknown until recently despite the fact that a countless number of observational and qualitative studies had been conducted. In order to develop the artificial baroreflex system, i.e., the bionic baroreflex system, we first anatomically isolated the carotid sinuses to open the baroreflex loop and identified the open-loop transfer function of the baroreflex system using white noise pressure perturbations. We found that the baroreflex system is basically a lowpass filter and remarkably linear. As an actuator to implement the bionic baroreflex system, we then stimulated the sympathetic efferent nerves at various parts of the baroreflex loop and identified the transfer functions from the stimulation sites to systemic arterial pressure. We found that the actuator responses can be described remarkably well with linear transfer functions. Since transfer functions of the native baroreflex and of the actuator were identified, the controller that is required to reproduce the native baroreflex transfer function can be easily derived from those transfer functions. To examine the performance of bionic baroreflex system, we implemented it animal models of baroreflex failure. The bionic baroreflex system restored normal arterial pressure regulation against orthostatic stresses that is indistinguishable from the native baroreflex system.**

I. Introduction

Baroreflex is known to be the fastest mechanism in the body to stabilize arterial pressure. The reflex makes use of negative feedback mechanism. The baroreceptors sitting in the arterial wall sense arterial pressure and send the pressure signal to the brainstem through the afferent nerve fibers. The brainstem receives the pressure signal and judges the level of arterial pressure. If the level is low, the brainstem activates the sympathetic system innervating the heart and vascular system to increase arterial pressure. If the level of arterial pressure is high, the brainstem withdraws the sympathetic activation.

The baroreflex system is critically important in animal, particularly in human. This is because, unlike animals with four legs, the position dependent gravitational effect on circulation is most prominent in human. It is well known that once we lose the normal function of baroreflex, we no longer keep sitting and/or standing positions because of position induced profound hypotension and hypoperfusion of the brain. Baroreflex failure destroys normal life and is a devastating pathological state in human. However, since the baroreflex failure is a disease of the neural system, no effective treatment has ever developed to save those patients.

Baroreflex failure could happen under various conditions. In some patients, they lost baroreflex function because they have problems in the baroreceptors, the brainstem and/or the spinal cord. In those patients, if we can develop a mechanism to activate their sympathetic efferent system in response to changes in arterial pressure just like the native brainstem does, in theory, normal baroreflex function can be restored.

The purpose of this investigation is to develop an artificial baroreflex system, so called the bionic baroreflex system, to restore normal baroreflex function to overcome such a serious pathological condition.

II. Bionic Baroreflex System

Shown in Fig. 1 are how we identify the transfer function of the controller of bionic baroreflex system. First we identify the transfer function of the baroreflex open loop (H_{NATIVE}) from baroreceptor pressure to arterial pressure responses. We then electrically stimulate a particular site in the baroreflex loop and identify the transfer function of the actuator from the stimulation to arterial pressure responses ($H_{STM-AOP}$). Since the controller will be in series with the actuator, the transfer function of bionic baroreflex system becomes identical to the native baroreflex system when the transfer function of controller (H_{BIONIC}) satisfies the following equation:

$$H_{NATIVE} = H_{BIONIC} \times H_{STM-AOP}$$

In theory both H_{NATIVE} and $H_{STM-AOP}$ can be experimentally determined. Therefore, H_{BIONIC} can be determined. However whether such a simple approach works or not highly depends on the simplicity of the native baroreflex system including the system linearity. We therefore examined the dynamic characteristics of baroreflex system.

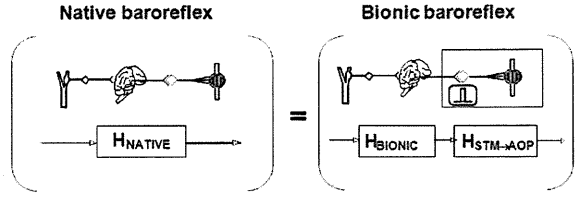

Fig. 1 Native vs. Bionic baroreflex

We vascularily isolated the baroreceptors (carotid sinuses) in rats (n=10) to open the baroreflex feedback loop and connected the carotid sinuses to a servo-controlled piston pump. This preparation allowed us to manipulate the carotid sinus pressure (CSP) independent of arterial pressure. We then perturbed CSP with random binary pressure sequences and identified the transfer function from CSP to arterial pressure. Shown in the left panels of Fig. 2 are the time series of CSP and aortic pressure. As can be seen, aortic pressure changes slowly toward the opposite direction in response to changes in CSP. This becomes even more evident in the transfer function (the right panel). The transfer function has low-pass filter characteristics. The phase response becomes nearly out-of-phase in the low frequency range suggesting the negative feedback nature of baroreflex system. Note that the magnitude squared coherence function is about 0.8 over the frequency range of interest. This is to say that most dominant characteristics of the total baroreflex open loop are captured by the linear transfer function.

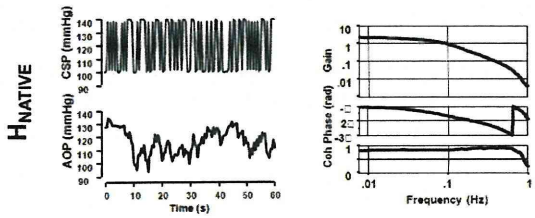

Fig. 2 Dynamic characteristics of native baroreflex system

In order to identify the actuator transfer function, we electrically stimulated the celiac ganglia with random binary pressure perturbations. Illustrated in the left panels of Fig. 3 are the time series of stimulation of celiac ganglia and aortic pressure responses. As can be seen, aortic pressure changes slowly toward the same direction in response to changes in stimulation. As anticipated the transfer function (the right panel) has low-pass filter characteristics. Unlike the total baroreflex loop, however, the phase response becomes nearly in-phase in the low frequency range. The magnitude squared coherence function is about 0.8 over the frequency range of interest. Again, it is reasonable to assume that most dominant characteristics of the actuator are captured by the linear transfer function.

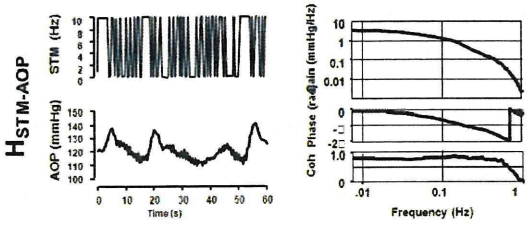

Fig. 3 Dynamic characteristics of sympathetic stimulation

We identified the transfer function (H_{BIONIC}) required for the controller by taking the ratio of H_{NATIVE} to $H_{STM-AOP}$. Since both dynamic characteristics of the total baroreflex loop and actuator are well represented by the linear transfer functions, the resultant H_{BIONIC} should reproduce the native characteristics of the baroreflex system when the feedback loop is closed. Shown in Fig. 4 are the changes in arterial pressure in response to orthostatic stresses under the open-loop baroreflex condition (baroreflex failure), the closed-loop baroreflex condition (native baroreflex) and the bionic baroreflex condition. Orthostatic stresses profoundly lowered arterial pressure in the absence of the native baroreflex. Closing the native baroreflex loop markedly attenuated the hypotensive responses. The activation of bionic baroreflex system also attenuated the hypotensive response as much as the native baroreflex system did. Statistical analysis indicated that the pressure regulation achieved by the bionic baroreflex system was indistinguishable from that achieved by the native baroreflex system.

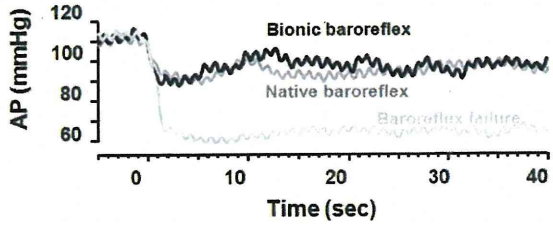

Fig. 4 Native baroreflex system vs. bionic baroreflex system

III. Discussion

We have shown that the bionic baroreflex system was as good as the native baroreflex system in regulating arterial pressure. The dynamic pressure responses to orthostatic stresses were indistinguishable between the native baroreflex system and the bionic baroreflex system. Although the baroreflex system is known to be nonlinear over the wide pressure range, we found that it is remarkably linear in the physiological pressure range. Because of this, the linear transfer function could represent the dominant characteristics of the baroreflex loop, and thereby allowed us to develop the bionic baroreflex system.

We can think of many anatomical sites where we can manipulate the activity of sympathetic system. In 1992, we stimulated the carotid sinus nerve to control the sympathetic system [1]. In 2004, we stimulated the spinal cord to stimulate the sympathetic efferent fibers [2]. The bionic mechanism worked beautifully regardless of the site of stimulation. It equally worked well in rats [3], rabbits [2], and dogs [1]. Although our experience of baroreflex failure in patients is limited, judging from its robustness, the bionic baroreflex system would work in patients as well [4]. If the bionic baroreflex system works in patients, it has a major impact as the treatment of baroreflex failure [5] that has been considered to be an incurable devastating disease.

IV. Conclusion

The bionic baroreflex system restores normal baroreflex function in an animal model of baroreflex failure.

ACKNOWLEDGMENT

This study was supported in part by Health and Labour Sciences Research Grant for Research on Medical Devices for Improving Impaired QOL from the Ministry of Health Labour and Welfare of Japan, Health and Labour Sciences Research Grant for Clinical Research from the Ministry of Health Labour and Welfare of Japan, and Grant-in-Aid for Scientific Research(S) (18100006) from the Japan Society for the Promotion of Science.

REFERENCES

[1] T. Kubota, H. Chishaki, T. Yoshida, K. Sunagawa, A. Takeshita, and Y. Nose, "How to encode arterial pressure into carotid sinus nerve to invoke natural baroreflex," *Am J Physiol* 263: H307-H313, 1992

[2] Y. Yanagiya, T. Sato, T. Kawada, M. Inagaki, T. Tatewaki, C. Zheng, A. Kamiya, H. Takaki, M. Sugimachi, and K. Sunagawa, "Bionic epidural stimulation restores arterial pressure regulation during orthostasis," *J Appl Physiol* 97: 984-990, 2004

[3] T. Sato, T. Kawada, T. Shishido, M. Sugimachi, and K. Sunagawa, "Novel therapeutic strategy against central baroreflex failure: A bionic baroreflex system," *Circulation* 100: 299-304, 1999

[4] F. Yamasaki, T. Ushida, T. Yokoyama, M. Ando, K. Yamasaki, and T. Sato, "Artificial baroreflex: clinical application of a bionic baroreflex system," *Circulation* 113: 634-639, 2008

[5] M. Sugimachi, and K. Sunagawa, "Bionic cardiology: exploration into a wealth of controllable body parts in the cardiovascular system," *IEEE Rev Biomed Eng.* 2: 172-186, 2009.

32nd Annual International Conference of the IEEE EMBS
Buenos Aires, Argentina, August 31 - September 4, 2010

Physiological Significance of Pressure-Volume Relationship: a Load-Independent Index and a Determinant of Pump Function

Masaru Sugimachi, *Member, IEEE*, Kenji Sunagawa, *Member, IEEE*,
Kazunori Uemura, and Toshiaki Shishido

Abstract—**Pressure-volume relationship permits conceptual integration with time-varying elastance, stress-strain relationship, and pressure-volume area. It has also superior usefulness to other indexes, both as a load-independent index of ventricular contractility and as a determinant of ventricular pump function.**

PRESSURE-VOLUME relationship has become a standard framework [1] for discussing the mechanical properties of the ventricles and sometimes atria. It has gained popularity because of its conceptual integration and its superior usefulness, both as a load-independent index and as a determinant of pump function. The concept of pressure-volume relationship agrees with to that of time-varying elastance, that of (time-varying) material properties of myocardium (i.e., stress-strain relationship), and that of pressure-volume area as the major determinant of myocardial oxygen consumption [2].

A. A Load-Independent Index

Pressure-volume relationship (PVR), especially the end-systolic pressure-volume relationship (ESPVR), has been repeatedly shown as one of the least load-sensitive index of ventricular contractility. Although preload-recruitable stroke work (PRSW) has been a rival, it is obvious that PRSW would no longer be load insensitive in extreme cases such as isovolumic beats.

Although detailed examination of ESPVR revealed its load-dependence (such as deactivation and activation associated with ejection) and curvilinearity [3], ESPVR is still the least load-dependent index of ventricular contractility. The apparent linearity of ESPVR seems to be observed just by chance, taking into consideration that ESPVR can be reconstructed from nonlinear (exponential) end-systolic stress-strain relationship of myocardium.

The most important advance what the concept of PVR has provided are the decoupling of heart from vasculature (preload and afterload), and the fact that actively contracting tissue would change its mechanical properties in cardiac cycles. Decoupling the heart enabled us to separately discuss the changes in the heart and the vasculature, rather than mix them and discuss only the measured hemodynamic variables. The uncovered complex load-dependence and curvilinearity would have not sacrificed the value of decoupling. The concept of changeable material property has simplified the explanation of complex time course of pressure development and ejection.

B. A Determinant of Pump Function

ESPVR has provided a method to precisely predict the stroke volume for given end-diastolic volume, heart rate and afterload resistance. This was accomplished by recoupling ESPVR with effective arterial elastance (mainly determined by heart rate and resistance). This is a major advantage over PRSW. What is more, even the pressure and flow waveform can be reconstructed by recoupling time-varying PVR (for the entire cardiac cycle) and arterial high-resolution impedance [4].

Manuscript received April 7, 2009. This work was supported in part by Grant-in-Aid for Scientific Research (B 20300164) from the Ministry of Education, Culture. Sports, Science and Technology, by Health and Labour Sciences Research Grants (H20-katsudo-shitei-007) from the Ministry of Health Labour and Welfare of Japan.

M. Sugimachi, K. Uemura, and T. Shishido are with the National Cardiovascular Center Research Institute, Suita, Osaka 5658565, Japan (corresponding author Masaru Sugimachi to provide phone: +81-6-6833 -5012; fax: +81-6-6835-5403; e-mail: su91mach@ri.ncvc.go.jp).

K. Sunagawa is with Kyushu University, Fukuoka 8128582 Japan. (e-mail: sunagawa@cardiol.med.kyushu-u.ac.jp).

REFERENCES

[1] K. Sagawa, L. Maughan, H. Suga, and K. Sunagawa, "Cardiac Contraction and the Pressure-Volume Relationship," New York, Oxford University Press, 1988.

[2] H. Suga, "Ventricular energetics," *Physiol. Rev.* vol. 70, no. 2, 247–277, Apr. 1990.

[3] D. Burkhoff, S. Sugiura, D. T. Yue, and K. Sagawa, "Contractility-dependent curvilinearity of end-systolic pressure-volume relations," *Am. J. Physiol.* vol. 252, no. 6, part 2, H1218–H1227, Jun. 1987.

[4] T. W. Latson, W. C. Hunter, D. Burkhoff, K. Sagawa, "Time sequential prediction of ventricular-vascular interactions," *Am. J. Physiol.* vol. 251, no. 6, part 2, H1341–H1353, Dec. 1986.

32nd Annual International Conference of the IEEE EMBS
Buenos Aires, Argentina, August 31 - September 4, 2010

Estimated Venous Return Surface and Cardiac Output Curve Precisely Predicts New Hemodynamics after Volume Change

Masaru Sugimachi, *Member, IEEE*, Kenji Sunagawa, *Member, IEEE*,
Kazunori Uemura, Atsunori Kamiya, Shuji Shimizu, Masashi Inagaki and Toshiaki Shishido

Abstract— **In our extended Guyton's model, the ability of heart to pump blood is characterized by a cardiac output curve and the ability of vasculature to pool blood by a venous return surface. These intersect in a three-dimensional coordinate system at the operating right atrial pressure, left atrial pressure, and cardiac output. The baseline cardiac output curve and venous return surface and their changes after volume change would predict new hemodynamics. The invasive methods needed to precisely characterize cardiac output curve and venous return surface led us to aim at estimating cardiac output curve and venous return surface from a single hemodynamic measurement. Using the average values for two logarithmic function parameters, and for two slopes of a surface, we were able to estimate cardiac output curve and venous return surface. The estimated curve and surface predicted new hemodynamics after volume change precisely.**

I. Introduction

OUR group has developed an extended Guyton's cardiovascular model, where the ability of the right- and left-sided heart to pump blood is integratively characterized by a single curve (cardiac output curve) and the ability of vasculature to pool blood is expressed as a surface (venous return surface). The cardiac output curve and the venous return surface intersect in a three-dimensional coordinate system, and the three coordinates show the operating right atrial pressure (RAP), left atrial pressure (LAP), and cardiac output (CO), respectively (Fig. 1).

If one knows the baseline cardiac output curve and venous return surface and how these change after volume infusion and depletion, one can predict new hemodynamics by combining a new cardiac output curve and a new venous return surface. The precise characterization of cardiac output curve and venous return surface, however, needs extremely invasive measures for changing loading conditions to be applicable to patients with heart diseases (see Sections IIB and IIC for the detailed invasive methods used in animal experiments). Therefore, the aim of this study was to circumvent this difficulty by establishing a method to approximately obtain the cardiac output curve and venous return surface from a single hemodynamic measurement.

Manuscript received April 7, 2009. This work was supported in part by Grant-in-Aid for Scientific Research (B 20300164, C 20500404) from the Ministry of Education, Culture, Sports, Science and Technology, by Health and Labour Sciences Research Grants (H20-katsudo-shitei-007) from the Ministry of Health Labour and Welfare of Japan.

M. Sugimachi, K. Uemura, A. Kamiya, S. Shimizu, M. Inagaki and T. Shishido are with the National Cardiovascular Center Research Institute, Suita, Osaka 5658565, Japan (corresponding author Masaru Sugimachi to provide phone: +81-6-6833-5012; fax: +81-6-6835-5403; e-mail: su91mach@ri.ncvc.go.jp).

K. Sunagawa is with Kyushu University, Fukuoka 8128582 Japan. (e-mail: sunagawa@cardiol.med.kyushu-u.ac.jp).

II. Model and Methods

A. Extended Guyton's Model

We have extended Guyton's model [1] to handle a number of difficulties frequently encountered in clinical settings in patients with predominantly unilateral heart failure.

First, we extended a 2D (RAP-CO) Guyton's model to a 3D (RAP-LAP-CO) model, and introduced a third axis for LAP (Fig. 1) [2], [3]. By this modification, we can get the operating LAP directly from the intersection between cardiac output curve and venous return surface. LAP indicates the degree of pulmonary congestion and inadequate blood oxygenation, and normal range of LAP is as important as that of cardiac output and that of blood pressure for sustaining life.

Second, in this 3D model, we can separately express the changes in pumping ability of the right- and left-sided heart; the 3D cardiac output curve (Fig. 1, thick curve) is, in reality, the integration of two separate 2D cardiac output curves. The pumping ability of the right-sided heart can be obtained by projecting the 3D curve to the RAP-CO plane, and that of the

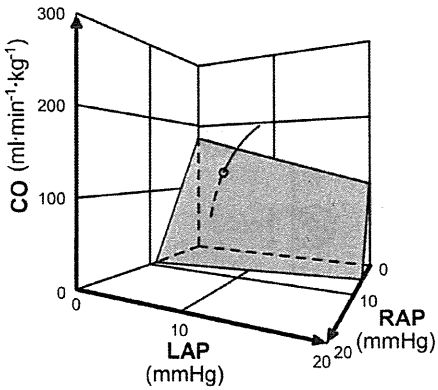

Fig. 1. An extended Guyton's model. The curve integratively expresses the pumping ability of right- and left-sided heart. The shaded surface characterizes the blood-pooling ability of the vasculature. RAP, right atrial pressure; LAP, left atrial pressure; CO, cardiac output (per kg of body weight).